Experimental characterization of velocity and acoustic fields of single-stream subsonic jets

Odenir de Almeida[1],

Experimental Aerodynamics Research Center – CPAERO, School of Mechanical Engineering, Federal University of Uberlandia - UFU, Uberlandia, Minas Gerais, Brazil

Anderson Ramos Proença, Rodney Harold Self

Institute of Sound and Vibration Research – ISVR, University of Southampton, Southampton, United Kingdom

[1] Author for correspondence

Abstract

The characterization of velocity and acoustic fields from a single-stream free jet operating at subsonic regimes is essential for aeronautical applications. For instance, the investigation of exhaust gases from single or coaxial nozzles or from bleed valve in turbojets and turbofan engines is crucial for understanding the mechanisms of noise generation and propagation and eventually for finding ways to reduce aircraft noise. This article evaluates the velocity and acoustic fields of an isothermal single jet discharging from a circular 38.1 mm conical nozzle at three different Mach and Reynolds numbers of 0.25 ($Re = 2.5 \times 10^5$), 0.50 ($Re = 4.9 \times 10^5$) and 0.75 ($Re = 6.8 \times 10^5$), respectively. Pitot-tube and hot-wire probes were used to identify the mean velocity profiles in longitudinal and transversal directions in the wake of the jet. The hot-wire anemometry system was also used to evaluate the turbulence intensity distribution over eleven axial lines, from the centerline to the edge of the nozzle. The accuracy of hot-wire anemometers for turbulent intensities lower than 15% at low and high subsonic Mach numbers was evaluated by comparing the experimental measurements with available data from the literature. An acoustic investigation was carried out by analyzing the sound pressure level obtained at six positions in the far field, with viewing angles ranging from 40° to 110°. The results were integrated to a database with sound pressure level as a function of Strouhal number, aiming to provide a benchmark for further RANS-based methods applied to aeroacoustic simulations of single jets.

Keywords

Aerodynamics; Aeroacoustics; Experimental; Jet noise; Aircraft noise; Hot-wire

1. Introduction

Air transportation is one of the safest travel modes nowadays. The number of daily flights is significant, and the number of air passengers has increased at a fast pace. The industry and research centers have focused on reducing aircraft noise, which has been a major concern in the aeronautical field since the introduction of jet-engine-powered aircrafts [1]. Studies have shown noise exposure, which is significantly burdened by traffic noise, has been the most undesirable feature in current urban life [1].

Fig. 1 shows the global trend of noise exposure to aircraft operation [2]. It plots the population in millions exposed to 55, 60 and 65 dB aircraft noise from year 2000 through 2025.

Fig. 2 shows an actual example of such exposure to aircraft noise at Congonhas Airport in Sao Paulo, Brazil, once the airport is surrounded by a very populated area subjected to approximately 600 daily flights.

Aircraft-emitted noise stems from several noise sources. Engines are one of the major noise sources on the ground, while fan and jet exhausts are the major noise contributors at take-off and climb. As a major concern in aeronautical applications, jet noise has been widely investigated. Driven by new noise regulations [4–5], the aeronautical industry and research

centers have made efforts to propose new techniques to reduce engine and consequently aircraft noise.

This article reports on an experimental study of free jets with a view to providing a benchmark to aid in the development of computational aeroacoustic methods oriented to jet noise reduction. Experimental research on the mean velocity profiles of free jets has been reported for at least one century, since the pioneer work of Trüpel [6], followed by Abramovich [7], Corrsin and Uberoi [8,9] and Hinze [10], among others.

At first, instrumentation usually relied on Pitot-tube probes, which were largely used to measure mean velocity profiles and some of the turbulence quantities in the free jet flow. Subsequently, hot-wire anemometry was introduced to obtain point-wise measurements of turbulent fluctuations and complete velocity fields [11–13]. Both Pitot-tube probes and hot-wire anemometers have been used to measure mean velocity fields, turbulent intensity and frequency spectra among other quantities in a jet flow field.

Pairs of hot-wire sensors have been used to define the size and shape of regions with correlated turbulent velocities. Measurements of space correlations at retarded times have been used to define, for instance, a convection velocity and then obtain spectra and time scales in the turbulence-moving frame [14–16]. Laser Doppler Velocimetry (LDV) and hot-wire probes have been used to obtain additional data on single-stream subsonic jets [17]. Hot-wire-only measurements have also been obtained in the work [18]. Further research has shown the effect of nozzle exit conditions on subsonic jet noise [19] and the importance of studying turbulent high-speed, single-stream jets for aeronautical applications.

From an acoustic perspective, jet noise can be obtained directly from using a set of microphones. Accurate instrumentation and facilities for jet noise measurements became available in the second half of 1980, providing a large amount of high-quality narrow-band jet noise data [20]. One of the main applications of acoustic measurements of free jets is building a database to predict jet noise by interpolating and extrapolating data, usually through a semi-empirical model. For example, ESDU 98019 [21] and SAE ARP 876D [22] are databases for single-stream jets obtained in different experiments, each with specific data for Strouhal number, temperature ratio, and observer angles.

Despite the importance of investigating jet noise, the lack of experimental data has been a major problem to research groups since mathematical and numerical models require benchmark for validation. As jet noise is a profit factor in the aeronautical industry, open source databases have not been widely available in the literature. The few available databases have not been adequately provided with their input parameters or else have featured restrictions to retrieve some of their parameters, including velocities and observer angles. Recent cooperation projects between universities and companies have addressed this problem, as is the case of the European Union research framework programs for new engine noise reducing technologies.

This article reports on a study developed within a consortium involving Embraer S.A. and 6 Brazilian universities co-associated with foreign partners. The consortium carried out two research projects from 2012 through 2015 aiming to develop expertise and methods for

aeroacoustic predictions of fan noise, airframe noise and jet noise. The main contribution of this work was to use Pitot-tube probe, hot-wire anemometry and far-field acoustic measurements to perform an experimental characterization of velocity and acoustic fields of single-stream subsonic jets operating at Mach 0.25, 0.50 and 0.75. The resulting data provided a better understanding of the flow dynamics and acoustic fields of such jets. The data have been used to validate ongoing numerical approaches to reducing jet noise with accuracy and at relatively low costs, which will eventually allow for the application of such techniques in the aeronautical industry.

2. Experimental arrangement

Measurements were performed at the Doak laboratory, a Rolls Royce University Technologic Center (UTC) facility located in the Institute of Sound and Vibration Research (ISVR) at University of Southampton, United Kingdom. The Doak laboratory is a 15 m × 7 m × 5 m fully anechoic chamber for frequencies down to 400 Hz. Its four walls, ceiling and floor were covered with wedge-type sound absorbing material. A non-forced exhaust system was built with a rectangular collector section allowing air to pass through into a small secondary acoustic chamber. The air flow was fed with 20-bar high-pressure compressed air from two storage tanks, and the velocity range available for testing was Mach 0.2–1. Fig. 3 shows the anechoic chamber with a nozzle and a hot-wire anemometer.

The test article was a 38.1 mm exit-diameter, convergent, conical nozzle used for most of the tests performed at the Doak Laboratory (Fig. 4).

A Pitot tube was used to measure mean velocity profiles in the jet flow to serve as a reference for the velocity inside the jet rig while calibrating the hot-wire sensors. Two different transducer systems coupled to the Pitot tube were used in the experiments: a Pitot-tube micro-manometer, allowing velocities up to 180 m/s, and a Druk PDCR 820 transducer. The data for each test point were acquired in an interval of 10 s. with a sample frequency of 1 kHz to perform Pitot-tube-based mean velocity survey. Fig. 5 describes the set of Pitot tubes used in such measurements.

A hot-wire anemometry system was used for mean flow and turbulence intensity measurements in the wake of the jet. The capability of the constant temperature anemometer (CTA) for measuring flow fields at high Mach number (above 0.30) was also checked during the tests. An acquisition frequency of 50 kHz was used throughout all measurements. Fig. 6 shows one of the single hot-wire anemometers used and the temperature probe setup.

A traverse system was used to move probes and sensors inside the jet flow. The system, an ISEL® traverse controller (Fig. 3), allowed 3-axis movements. It was manually or automatically moved by a remote control, and its positioning accuracy was approximately 0.5 mm. This device was compatible with the standard software provided by the manufacturer and could be connected to a computer via serial interface, allowing movement by coordinates or by a matrix of several predefined positions, which was useful for mapping inside the flow.

Far-field acoustics measurements were performed with ¼" GRAS® 40BF microphones with a frequency range of 10 Hz to 100 kHz and a dynamic range of 40–174 dB (reference 20 µPa) (Fig. 7). The microphone's normal sensitivity was 4 mV/Pa, which was checked before each experiment day. The preamplifiers were B&K Falcon Range ¼" 2670® with full electromagnetic compatibility. The microphones were powered by NEXUS® conditioning amplifier units with their HP filters set at 20 Hz.

Both a polar array and a transversal azimuthal array of microphones could be used to obtain a complete three-dimensional sound field in the Doak laboratory. Acoustic measurements were performed only for far field at six different observer angles. Background acoustic measurements were taken during each test session. The polar angles for far-field acoustics measurements were 40°, 50°, 60°, 75°, 90° and 110°. The acquisition frequency for the acoustics measurement was 100 kHz.

The ¼" condenser microphones were mounted in the same plane as the jet axis. The stands were placed in such a way that the microphones were parallel to the jet axis (Fig. 8). The distances between the center of the exit nozzle and the microphones were corrected to 1 m. The microphones were orientated at 0° incidence, i.e., pointing to the center of the nozzle.

Initially, a test matrix was built for the aerodynamics measurements including mean velocity, turbulent intensity profiles and turbulence spectrum energy. The aerodynamics experiments were carried out to obtain measurements as follows: mean velocity profile from a Pitot-tube probe and a single hot-wire anemometer, turbulent intensity from a one-component hot-wire anemometer, turbulent intensity from a three-component hot-film anemometer, and turbulent spectrum energy from a triple sensor hot-film anemometer. The acquisition frequency for each sensor was 1 kHz for Pitot-tube probes and 50 kHz for hot-wire probes.

Mean velocity distributions were acquired along the jet axis to different radial positions (Fig. 9). The center of the nozzle was on "0," and vertical axis 'y' represented radial variation to the nozzle radius while 'x' represented the jet axis. "Red" points symbolized data acquisition positions. Points within the grey rectangle were acquired only from single hot-wire probes. A matrix of coordinates was used to move the traverse system automatically and obtain all the points to each prescribed Mach number.

Fig. 10 shows a sketch containing the measuring lines used by the traverse system to acquire the test points. Measurements started with the velocity acquisition by the hot-wire anemometry system in the centerline (C-line) of the jet at the coordinate (0, 0). Data acquisition started at the relative location x/Dj=0, and then the traverse moved downstream the jet, until reaching x/Dj=13, the maximum position in the x-line. This procedure was repeated for all C-lines, from C1 to C-lip (i.e., longitudinal line in the edge of the nozzle, namely the lip line). Between C-line and C-lip were 9 intermediate lines spaced by 1.905 mm from each other in the y-direction. Thus, C1 represents the longitudinal line at y/Dj = 0.05 and so on up to C-lip at y/Dj = 0.5. Finally, Pitot-tube probes also collected 20 lines beyond the lip line, namely from (S1) to (S20).

The point-location matrix (Fig. 9) contained a total of 963 points from Pitot-tube probes and 593 points from hot-wire probes. Such data were used to create mean velocity contours, which served to characterize the wake flow. Point-wise velocity measurements, obtained by half diameter, were mirrored to complete the velocity profiles and the contour plots under the assumption of jet axisymmetry.

3. Aerodynamics results

This section first reports the results for axial and radial velocity profiles. Then it introduces the contour plots for the jet's wake characterization and the turbulent intensity graphs. Finally, it presents the power spectrum density (PSD). The results were obtained for a single isothermal jet under 0.25, 0.50 and 0.75 Mach conditions and respective Reynolds numbers of 2.5×10^5, 4.9×10^5 and 6.8×10^5.

Fig. 11 shows the Pitot-tube results for velocity distribution along different C-lines within the nozzle region from the centerline (C-line) to the edge of the nozzle (C-lip). For brevity, only a group of 6 C-lines were provided for each Mach number investigated. Each line was normalized independently by dividing velocity (U) by the maximum velocity (Umax) measured along each specific line. The potential core ended between 4 and 4.5 diameters downstream the jet axis, as represented by the values obtained in centerline (C-line) for all Mach conditions analyzed.

The plots also showed a satisfactory trend in the Pitot-tube measurements. Minor peaks were found in the curves when the probe was moved outside the potential core region. Since the potential core has a statistical characteristic of a conical shape, the greater the distance from the centerline, the higher the velocity decay, as seen in the curves from C2 to Clip, which consistently repeated in Fig. 11(a)–(c). However, even considering all measurements were corrected to the flow variation, there was a single discrepancy represented by the C-line and C2 data in Fig. 11(a). In that case, the data from C2 line represented a longer potential core, which in fact is not true. This difference was attributed to an instantaneous flow velocity increase, probably related to increased pressure in the compressor for an unknown reason during measurement. A decision was made to maintain these data in the database to show the sensitivity of this kind of measurement. Despite this difference between C2 and C-line for Mach 0.25 flow, the plots were consistent with the conditions observed; the potential core length and the trend along the axial lines were very similar for Mach 0.50 and 0.75, with the size increasing as the Mach number increased.

The same sequence of measurements was performed using a hot-wire sensor (Fig. 12). High velocity fluctuations above the lip line were identified, providing curves that were not as smooth as those found in the Pitot-tube data in Fig. 11. The constant temperature anemometer probe's response to convective cooling was accounted for as a calibrated probe was used. In this case, the non-linearities of the sensor increased where the turbulence intensity was higher and therefore the C-lip lines were removed from the plots in Fig. 12.

The Pitot-tube data presented much smoother curves for the velocity distribution along the C-lines than the hot-wire data. As the post-processed results had to be corrected to the

unsteady pressure imposed by the compressor system, the accumulated errors were more evident in the anemometry system. A sudden variation in the data was found in the C2 line for Mach 0.75 when reaching x/Dj = 12, as shown in Fig. 12(c), with an increase in the local velocity. As this trend was not observed in the Pitot-tube data (Fig. 11), a change in the pressure system was assumed to have caused such a fluctuation in the velocity field. In fact, a check in the compressor system functioning identified a fluctuation in the upcoming flow due to the activation of the compressor to supply air at high Mach numbers.

A striking result was the U-velocity decay below Uj, which was more evident in the centerline (C-line) for M = 0.50 and M = 0.75 plots in Fig. 12. This unexpected trend in the stream-wise velocity was attributed to the high sensitivity of the hot-wire sensor when applied to high turbulent flows and some calibration loss during high-speed flow measurements (M > 0.50). Such calibration loss is discussed later in this article when the present data are compared to those in the literature.

To check the trend and the accuracy of the data showed in Figs. 11 and 12, the results were compared against those reported by Morris and Zaman [16] (Fig. 13) and Jordan [17] (Fig. 14). An additional set of data was included to check the repeatability of the potential core sizing across different jet nozzles and experimental facilities. A word of caution should be added to Figs. 13 and 14: They refer to a general check, and as such neglect some of the variables and parameters necessary to such measurements.

Fig. 13 reveals the axial velocity profiles obtained in this work with the Pitot-tube probe were similar to those obtained through the hot-wire system. The exception was around 12 diameters, where the hot-wire results showed some inconsistency, as previously discussed. Despite the similarity between Pitot-tube and hot-wire data in this case, there was a difference in the values of the velocity distribution curve from [16]. Besides, the size of the potential core measured by Morris and Zaman [16] was larger than the potential core in the current measurement, and the authors used a different nozzle and experimental apparatus from those used in this analysis. Given such differences, the present comparison is only intended to check the sensitivity of velocity measurements in the jet's wake, pointing to variation in the measured data.

The results for Mach 0.75 were compared to those reported by Jordan [17] (Fig. 14). In this case, an offset was evident between the hot-wire probe and the Pitot-tube result. The Pitot-tube measurements agreed very well with the results found by Jordan [17], who obtained his measures with an LDV system, which allowed axial and radial local point measurements through the jet's wake. Since an increase in the length of the potential core was expected for a higher Mach number [14] in the present study, the conclusion was that the hot-wire probes may contain some source of error, which could be associated with the sensitivity of such a sensor to high turbulence flow or even a calibration loss during this specific measurement. In the post-processing, especially for Mach numbers 0.5 and 0.75, an offset was observed among several calibration curves of the sensor during the tests. This offset seemed to start at four diameters downstream the nozzle exit, reaching its peaks around seven diameters, and decreased until the last point measured in this study. This observation

points to the fragility of the modern hot-wires probes, with high frequency response, for measuring unsteady high subsonic flows.

The normalized mean stream-wise-velocity distribution along longitudinal lines also allowed the comparison of the velocity profiles from the different Mach numbers investigated, as shown in Fig. 15. The velocity profiles were extracted from the lines C1, C4, C7, and C-lip for the Pitot-tube probes, wherever they confirmed an increase in the jet's Mach number had led to an increase in the length of the potential core. Lau and Tester [24] showed the potential core comes to an end because the large-scale vortex pattern within the mixing region converges on the jet centerline during its travel downstream. Higher vortex convection is believed to exist in higher velocities, and this would result in the jet centerline displacement to greater distances downstream.

Figs. 16 and 17 show radial velocity profiles at different axial positions (x/Dj) in a Mach 0.50 jet as acquired with Pitot-tube and hot-wire probes, respectively. These curves were normalized by (Umax) selected under the proper radial line, thus providing peak values close to 1. Therefore, as expected, the velocity decayed with an increasing in the x-direction downstream the nozzle. This radial velocity profiles also showed the jet's spreading, since the profile was broadening in the y-direction. Results for Mach numbers 0.25 and 0.50 in this study followed the same trend.

As the hot-wire sensor collected fewer points than the Pitot tube and had them concentrated around half diameter in the y-direction (Fig. 8), the hot-wire curves were not as smooth as the Pitot-tube curves. Some small differences were also apparent in the peak values of the normalized velocity, which is consistent with those in Fig. 11(b) compared to Fig. 12(b). Increase in the Mach number led to accuracy loss in the hot-wire data, which showed a point-wise flow velocity that was lower than that observed in the Pitot-tube probe at the same location.

The Pitot-tube and the hot-wire points collected for all Mach numbers were used to create contour plots, showing the jet's flow pattern (Fig. 18). All lines measured in the jet's wake were considered, and the data were mirrored under the assumption of jet axisymmetry.

Fig. 18 clearly shows the potential core development and the shear layer spreading along the Mach number regimes. It points to a slight growth of the potential core with increased velocity. Although it seems to be merely illustrative or qualitative, it helped to summarize the information given from the velocity profiles. Fig. 18 is helpful to characterize the jet's wake and is a good visual reference for further Reynolds Averaged Navier-Stokes (RANS-based) data analysis.

Fig. 19 provides one-component turbulence intensity (u-velocity). The unsteadiness or fluctuation of "u" was approached as turbulence intensity by dividing the root-mean-square velocity (urms) by the measured velocity (U). According to hot-wire manufacturers, the reliable range for single hot-wire measurements is from 10 to 15% of the mean value. In

moving along the jet shear layer, the maximum turbulence intensity expected for a subsonic jet is around 15% [17].

The results shown in Fig. 19 relate the turbulence intensity distribution from the jet centerline to the lip line. Initially, the flow unsteadiness is very low, mainly before reaching three diameters from the nozzle. By moving radially from the centerline (C-line) to the lip line (C-lip), the turbulence intensity slightly increases and reaches its peak, since it is crossing the shear layer between the potential core and the mixing region moving from a laminar flow to the turbulent layer. In addition, with the end of the potential core, the transitional region arises and the unsteadiness of the velocity grows up in the centerline until around eight diameters, beginning the self-preserving or fully developed region.

The operational range of the hot-wire anemometer has total influence on the curve C-lip, since it is in the region of high turbulence. The data presented some inconsistency in the C8 and C-lip lines for Mach 0.50, which increased monotonically. Even in the previous lines (i.e., C4 and C6), the turbulence intensity experienced in the jet flows were too high for these very small and sensitive hot-wire probes. As previously noticed, some pressure oscillation was also identified in the compressor system during some measurements, causing local velocity variation. Another error source identified was the calibration loss of the hot-wire sensor at high subsonic conditions (M > 0.50). One of these factors or even a combination of them may have caused such variation in the data.

Fig. 20 shows the turbulence intensity distribution at the centerline for a jet operating at Mach 0.25 in this study and in Morris and Zaman [16]. Fig. 21 provides the same curves for a Mach 0.75 flow compared against the results reported by Jordan [17].

In Fig. 20 the hot-wire data were comparable to the measurements of Morris and Zaman [16], but clearly differed from those of Jordan [17]. A difference was noticed in the values at the nozzle exit, which could be associated with the main flow's residual turbulence. In Morris and Zaman [16], this value was around 1% while it was near 2% in the present study. However, the peak level was around 13.6% in both set of data, with misplacement in its location since the potential core size was larger in Morris and Zaman [16]. The hot-wire measurements seemed to be consistent for low-speed Mach numbers (below 0.30) in single-stream jets.

Contrastingly, Fig. 21 shows a clear mismatch between the data in this study and those reported by Jordan [17]. The residual turbulence at the nozzle exit was around 3% in Jordan's study [16], but around 2% in the present study. The turbulence intensity reached its maximum, 15% value, at downstream location around 9.5 diameter in Jordan's jet [17], while these values were around 12.5% at 6.5 diameter in this study. Given the non-linearities of the hot-wire sensor for high subsonic flows measurements (above 0.5), caution should be taken when considering the use of these sensors to assess such parameters as turbulence intensity and velocity fluctuations.

Finally, PSD is presented to show the strength of energy variation as a function of frequency. The results in Fig. 22 are related to measurements on the C9 line (y/Dj = 0.45) at different

axial (x/Dj) locations ranging from 0 to 12, for Mach numbers 0.25, 0.50 and 0.75, respectively.

The usual unit of PSD is energy per frequency, and the integral of the PSD over a given frequency range computes the average power in the signal. The spectra were calculated directly by a Fast-Fourier Transform method (FFT). The Welch's method was applied to calculate the PSD of the signal acquired by hot-wire probes. Fig. 22 shows PSD is consistent with the fundamental theory of jet noise, according to which the points inside the potential core have less energy than the points in the mixing layer. The low frequencies are responsible for the energy injection, whilst high frequencies dissipate energy. A characteristic peak "noise" consistently occurs in the PSD plots. Such an unexpected peak was also identified for the lowest velocity ($M < 0.30$), and it spread as the Mach number increased. The occurrence of such peak "noise" was most likely due to the nozzle vibration inside the chamber or flow interaction with the hot-wire anemometer support.

4. Far-field acoustics results

This section reports the far-field acoustics results, as obtained for all three Mach conditions, along the arc of microphones. All results were corrected for atmospheric attenuation, and the observer distance was 1 m for all angles. The frequency varied from 300 Hz, imposed by the anechoic properties of the chamber, to 80 kHz (although the sample frequency was 100 kHz, the filtering and post-processing took 80% of this value).

Fig. 23 shows the spectra of sound pressure level (SPL) for the microphone located at 90°, for all Mach numbers investigated. As an increase in the Mach number means a higher Reynolds number, with more turbulent structures and multiplicity of scales (flow with more energy), an increase was expected in the noise levels captured by the microphone. For low velocities ($M < 0.30$), an undesirable noise was observed at very high frequencies ($St > 5$). As noticed before, the occurrence of this high-frequency "noise" may have been associated with the insertions of the anemometer support within the flow and did not affect the spectra under 80 kHz.

Figs. 24 and 25 present the SPL for the angles 40° and 110°. Only the lowest and highest observer angles are shown because the velocity trend was well established for all cases investigated. Regardless of the observer angle, the fine-scale fluctuations and the large scale coherent structures fed by a flow with more energy should increase the SPL in all directions. When the observer is located at 90° or higher, these fine and large scales are not dominants in the noise produced. The SPL follow this trend for different velocities at the angles 40°, 50°, 60°, 75°, 90° and 110°.

Figs. 26–28 exhibit the SPL pattern as a function of the observer angle for the three Mach numbers (0.25, 0.50 and 0.75, respectively). Due to the sound directivity and the effects explained just before, the sound sources were convected downstream by the mean flow, and the maximum noise was radiated at observer angles between 30° and 50°. The SPL difference among the observer angles became higher at moderate Mach numbers (0.5) as the velocity increased.

Considering the overall sound pressure level (OASPL), other measurements were included in the analysis, all of which were obtained in the same facility with the same experimental apparatus and setup for Mach number from 0.1 to 1.0. Fig. 29 shows the same acoustics pattern as described previously, identifying an increase in the OASPL as the Mach number increased. The acoustic data obtained were consistent with other jet noise data available in closer Mach number regimes. These data will be applied in the near future to validate aeroacoustic tools under development in the research group.

5. Conclusions

This study aimed to tackle jet aerodynamics and acoustics through experimental techniques, exploring the basic related theory for three different Mach and Reynolds numbers M = 0.25 (Re = 2.5 × 105), M = 0.50 (Re = 4.9 × 105) and M = 0.75 (Re = 6.8 × 105). The primary objective was to compare results from Pitot-tube and hot-wire probes for low (M < 0.30) and high-speed (M > 0.50) subsonic jets to evaluate the sensitivity of the hot-wire anemometer in high-speed and turbulent flows. The secondary objective was to build a set of experimental data to be used as a benchmark for further numerical aeroacoustic simulations. Both velocity and acoustic investigation allowed some important considerations about these jets, especially when it came to the limitations of using hot-wire probes for characterizing high-speed jets. The turbulence intensities acquired with a single component hot-wire anemometer could confirm the well-established concept of the dissipation, initial range and fully developed regions, despite the constant occurrence of non-linearities in the data. The acoustic measurements showed the relation between sound intensity and jet velocity, reinforcing the fundamental theory.

In conclusion, modern hot-wire anemometer sensors have a high frequency response by featuring a reduced size, which is not attainable through other techniques. However, the system has an intrusive probe and is restricted to low-speed flows. During this study, the sensor was placed into high-speed flows (M > 0.50) and changed its properties in high velocities campaigns, losing calibration and restricting the accuracy of data. The hot-wire data were not completely unreliable, but should be considered with caution in instances of discrepancies. This result led the research group to look towards additional measurements techniques to improve data quality in the laboratory. This ongoing research into jet noise will continue with further assessment of length scale correlation, comparisons of turbulent kinetic energy spectrum obtained by triple sensor hot-film anemometer, correlation across curves from an SPL database as a function of Strouhal number, and use of other nozzles configurations.

Funding

This work was supported by Minas Gerais Research Foundation (FAPEMIG) [APQ-02270-2010].

Acknowledgements

The authors are thankful to the financial support from the Brazilian Coordination for the Improvement of Higher Education Personnel (CAPES) and Minas Gerais Research Foundation (FAPEMIG), as well as to the support from Institute of Sound and Vibration Research (ISVR) for the conclusion of one of the author's M.Sc. thesis. They are also thankful to Sao Paulo Research Foundation (FAPESP), Research Increment and Industrial Improvement Foundation (FIPAI) and EMBRAER S.A. for supporting projects "Silent Aircraft: An Aeroacoustic Investigation" and "Development of Improved Solutions through Aeroacoustic Tests for Aircraft External Noise", both developed in Brazil from 2010 through 2015.

References

[1] M. Smith Aircraft noise, Cambridge aerospace series, 3. Cambridge University Press, Cambridge, New York (1989)

[2] 7th USA/Europe Air Traffic Management R&D Seminar, Barcelona 2007. Trends in Global noise and emissions from commercial aviation for 2000 through 2025.

[3] Airport Spotting Blog. Spotting news for aircraft enthusiasts; 2016. http://www.airportspotting.com [accessed 14.06.16].

[4] International Civil Aviation Organization (ICAO): International Standards and recommended practices. Environmental protection. Annex 16 to the convention on international civil aviation, vol. I, 2nd edition. International Civil Aviation Organization; 1988.

[5] Federal Aviation Administration (FAA): from 1969 onwards, Federal Aviation Regulations (FAR), Part 36. Noise Standards: Aircraft Type and Airworthiness Certification, U.S. Department of Transportation (DOT), Washington D.C.

[6] T. Trüpel Über die Einwirkung eines Luftstrahles auf die umgebende Luft Oldenbourg, München (1914)

[7] G.N. Abramovich "The Theory of Turbulent Jets", edited by Leon H, The MIT Press Classics, Schindel (1963)

[8] Corrsin S, Uberoi MS. NACA TN no. 1865; 1949.

[9] Corrsin S, Uberoi MW. NACA Report no. 1040; 1951.

[10] J.O. Hinze "Turbulence". McGraw-Hill, New York (1959)

[11] Townsed A.A. "The structure of turbulent shear flow". Cambridge University; 1956.

[12] Laurence J.C. Intensity, scale and spectra of tarbulence in mixing region of free subsonic jet. NACA TR 1292; 1956.

[13] Lilley G.M. On the noise from air jets. Aero Res Counc, Lond, 20, 376-N. 40-F.M. 2724; 1958.

[14] P.O.A.L. Davies, M.J. Fisher, M.J. Barratt. The characteristics of the turbulence in the mixing region of a round jet. Department of Aeronautics and Astronautics, University of Southampton. (1962)

[15] Harper-Bourne M. Jet noise turbulence measurements. 9th AIAA/CEAS aeroacoustics conference and exhibit; 12–14 May 2003.

[16] P.J. Morris, K.B.M.Q. Zaman. Velocity measurements in jets with application to noise source modeling. J Sound Vib, 329 (2010), pp. 394-414

[17] Jordan P. Results from acoustic field measurements, project deliverable D3.6, JEAN-EU. In.: Framework Program, 5, 2002. Proceedings Ellipsis Poitiers: Laboratoire d'Etude Aerodynamiques; 2002. G4RD-CT-2000-00313.

[18] A.V.G. Cavalieri, P. Jordan, T. Colonius, Y. GervaisAxisymmetric superdirectivity in subsonic jets. J Fluid Mech, 704 (2012), pp. 388-420

[19] Zaman KBMQ. Effect of nozzle exit conditions on subsonic jet noise. 17th AIAA/CEAS aeroacoustics conference (32nd AIAA Aeroacoustics Conference), 2704; 2011.

[20] Tam CKW. Jet noise: since 1952. Theoret Comput Fluid Dynamics 1998;10:393–405. Department of Mathematics, Florida State University, Tallahassee; 1998.

[21] Engineering Science Data Unit – ESDU. Computer based estimation procedure for coaxial jet noise. Data Item 01004; 2001.

[22] Society of Automotive Engineers – SAE. Gas Turbine Exhaust Noise Prediction. Aerospace Recommended Practice ARP-876D; 1994.

[23] Proença AR. Experimental characterization of velocity and acoustic fields of single-stream subsonic jet. Thesis (M.Sc. thesis in Mechanical Engineering). Uberlândia: Federal University of Uberlandia; 2013.

[24] Lau JC, Tester BJ. An evaluation of the lighthill analogy for jet mixing noise generation: using LV turbulence, source location and spectral noise data. IUTAM/ICA/AIAA-Symposium Gottengen; 1979.

Figures

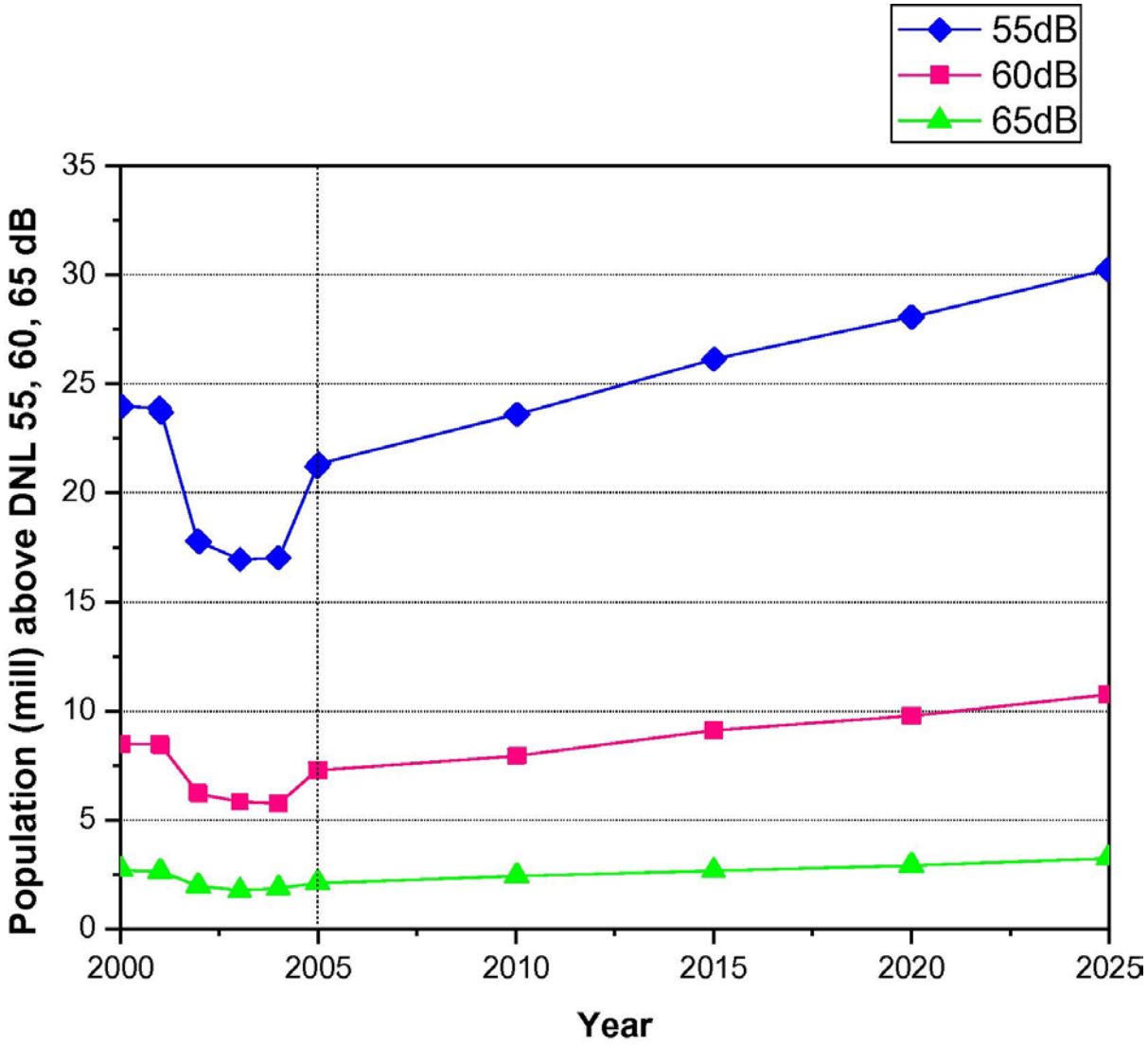

Fig. 1. Trend of exposure to aircraft operation. Source: [2].

Fig. 2. Congonhas Airport – Sao Paulo, Brazil. Source: [3].

Fig. 3. Overview of Doak Laboratory with a traverse system for hot-wire anemometry and Pitot-tube probes. Source: [23].

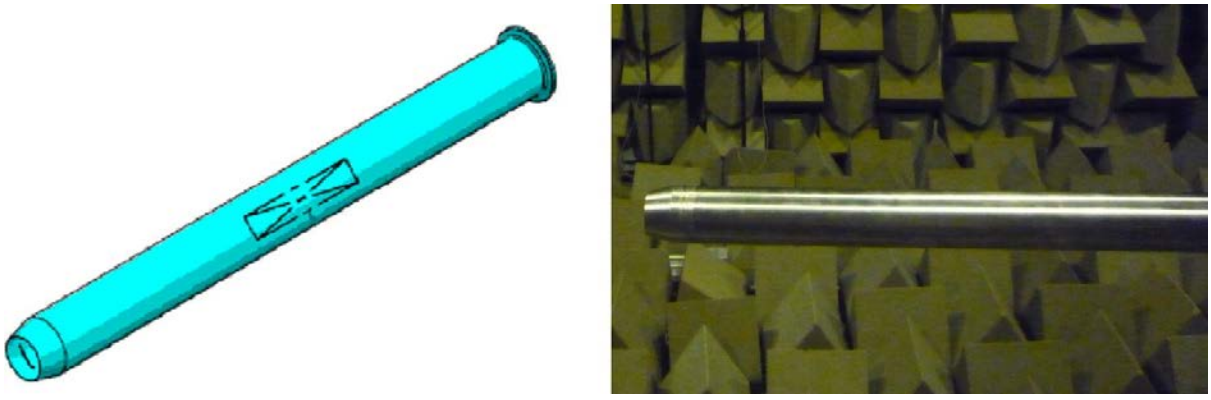

Fig. 4. Sketch and photo of the 38.1 mm reference conical nozzle. Source: [23].

Fig. 5. Different Pitot tubes used in the experiments. Source: [23].

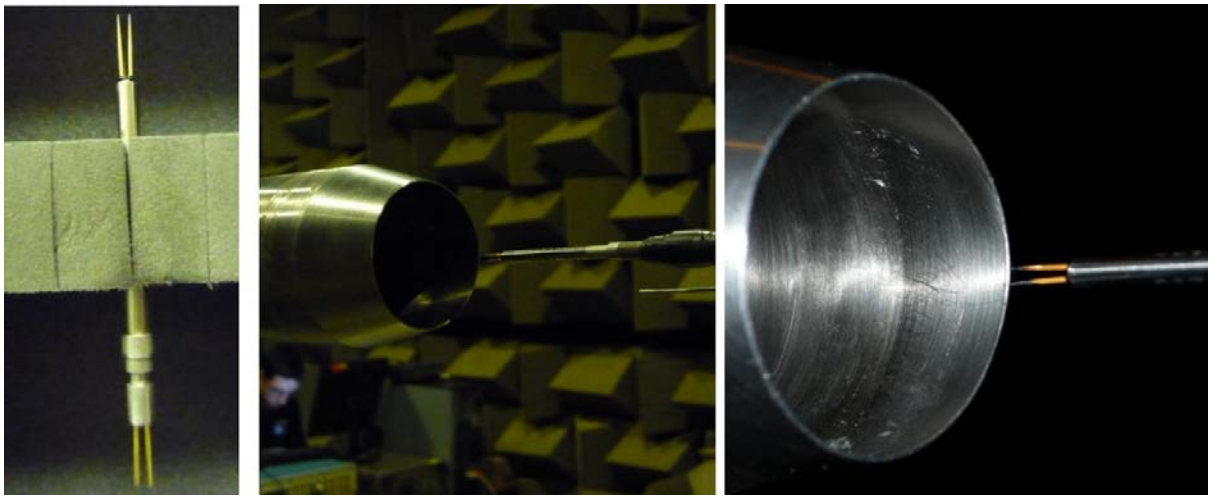

Fig. 6. Single hot-wire sensor applied in this work. Source: [23].

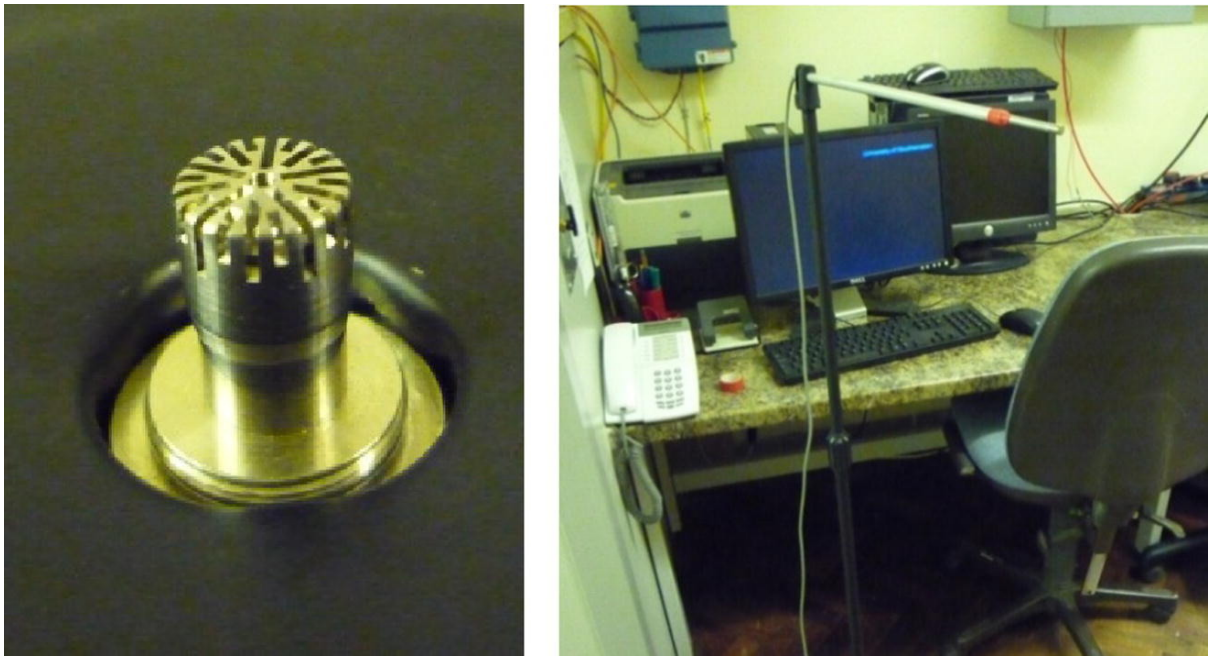

Fig. 7. ¼" GRAS 40BF microphone and its stand and preamplifier setup. Source: [23].

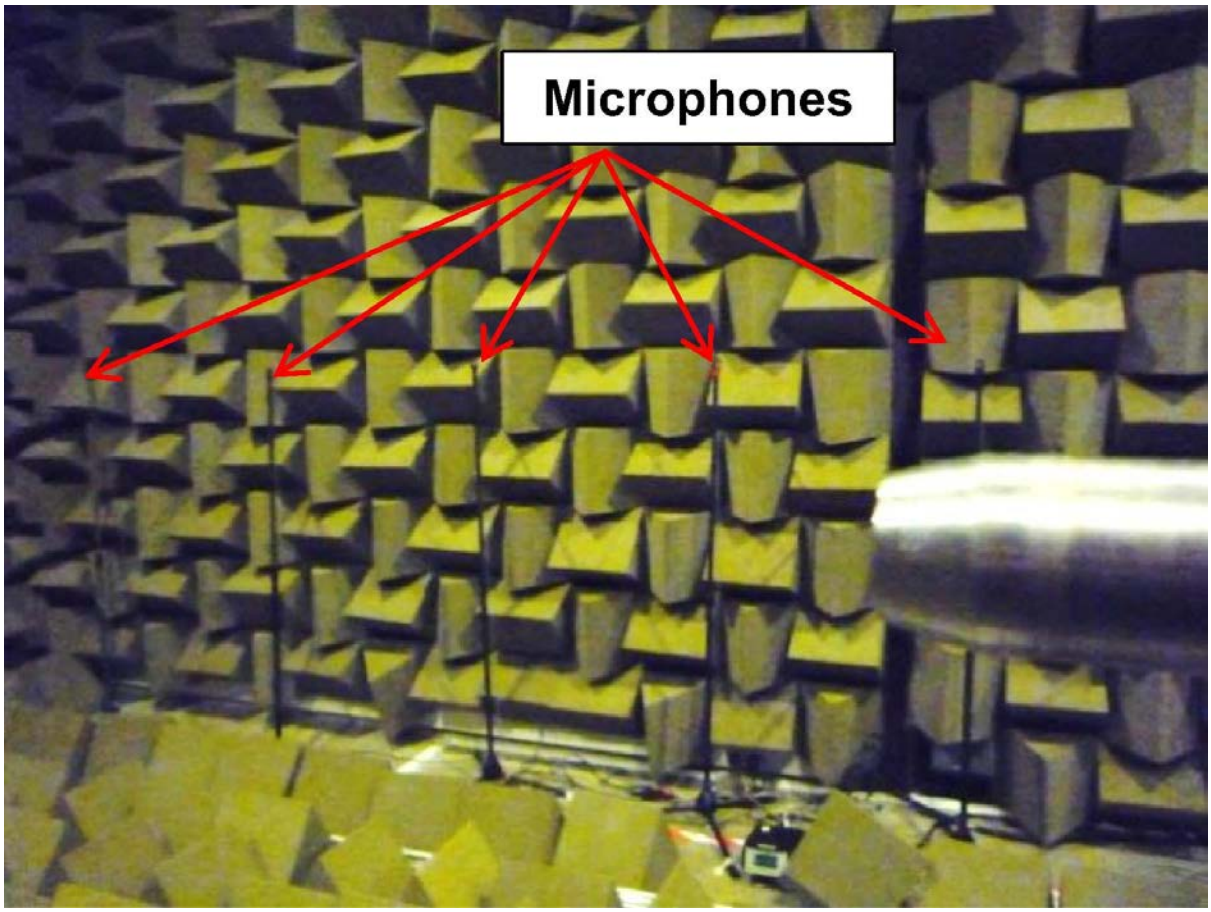

Fig. 8. Microphone positioning during acoustic measurements. Source: [23].

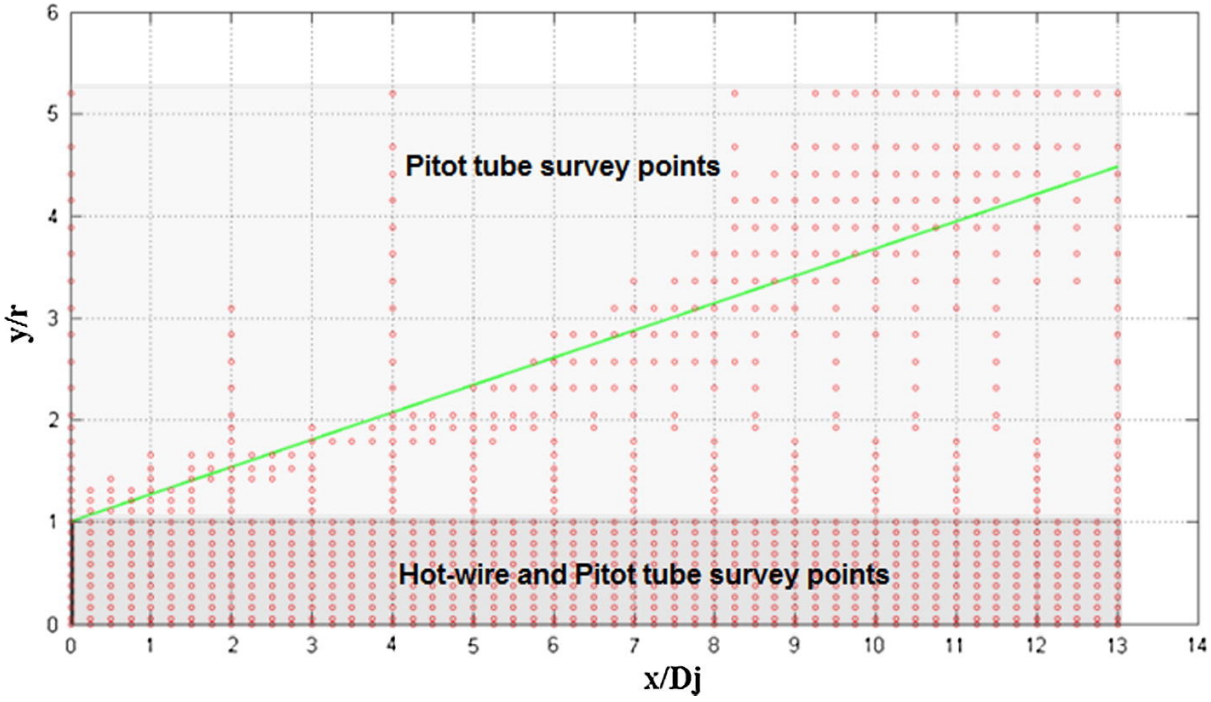

Fig. 9. Acquisition points of aerodynamics measurements along the jet region. Source: [23].

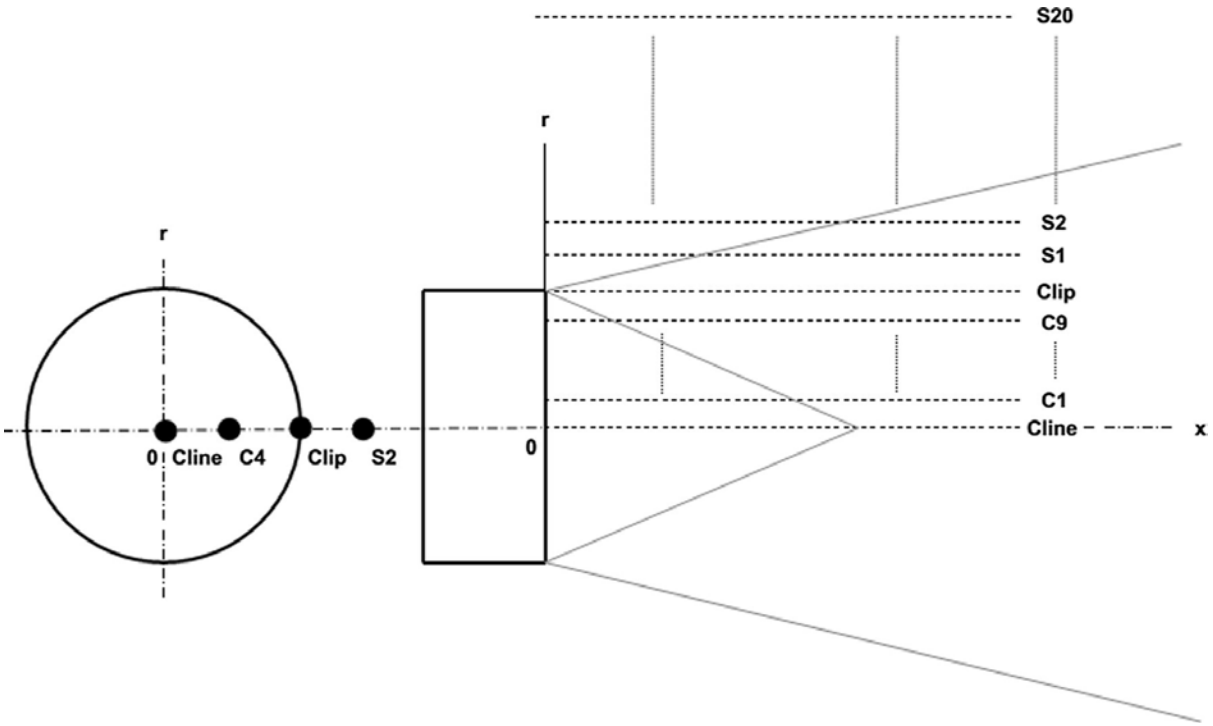

Fig. 10. Sketch of the lines for hot-wire (C-line) and Pitot-tube (S-lines) probes. Source: [23].

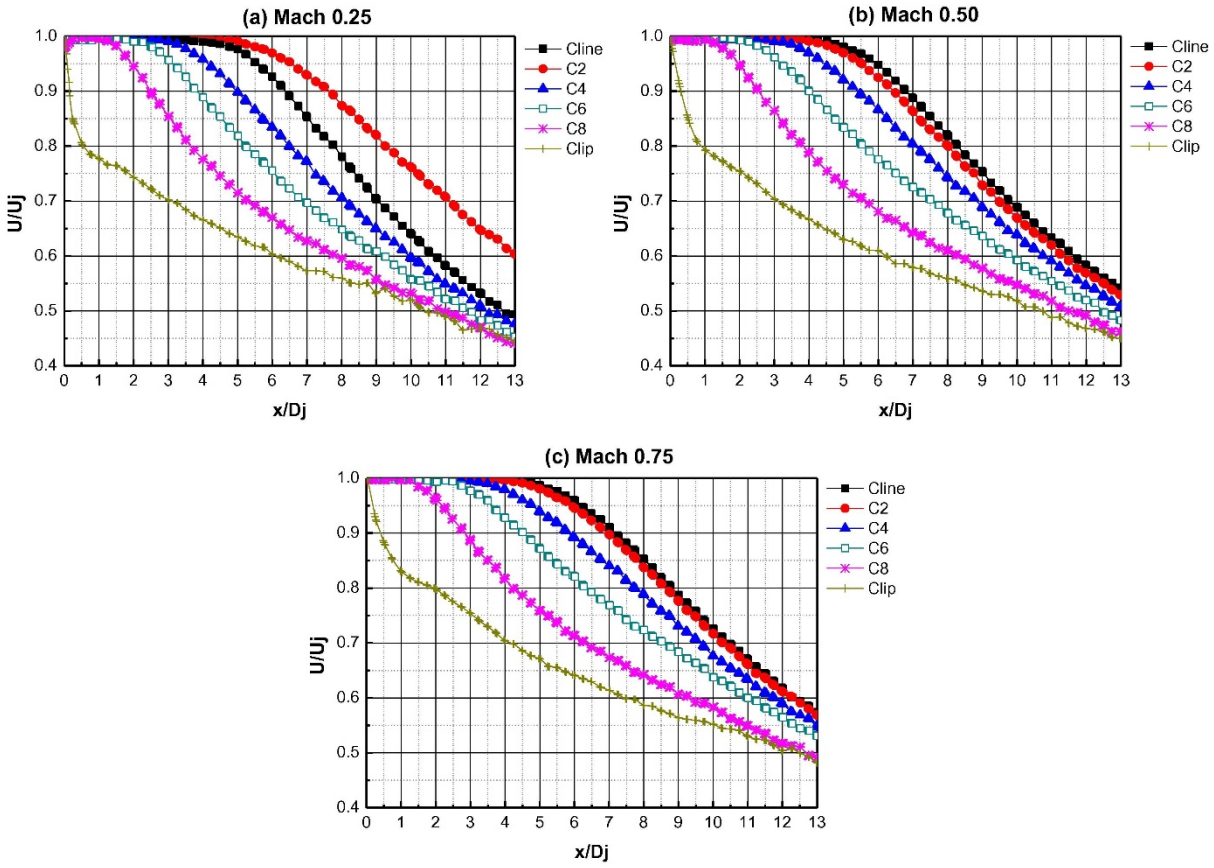

Fig. 11. Velocity distribution along the jet axis for different radial positions (C-lines), obtained through Pitot-tube for Mach 0.25 (a), 0.50 (b) and 0.75 (c), respectively.

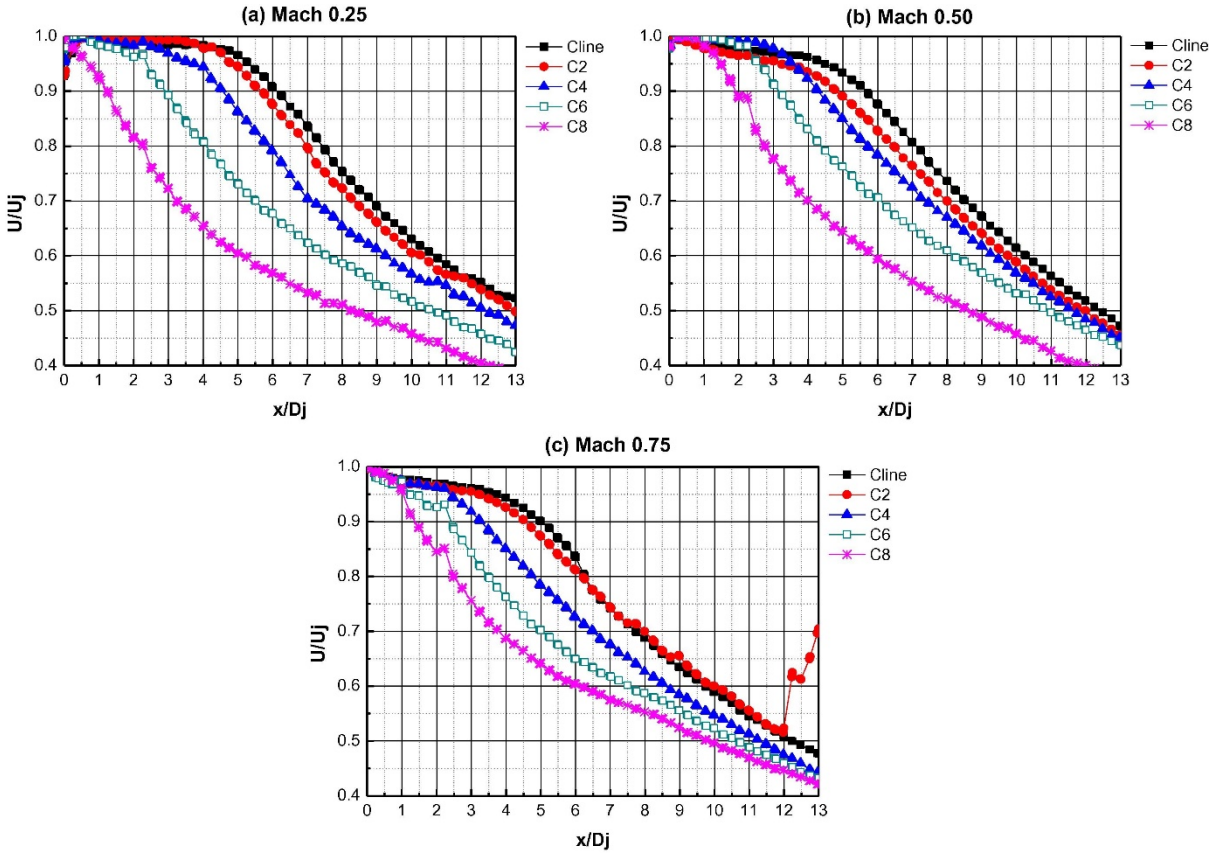

Fig. 12. Velocity distributions along the jet axis for different radial positions (C-lines), obtained through hot-wire probes for Mach 0.25 (a), 0.50 (b) and 0.75 (c), respectively.

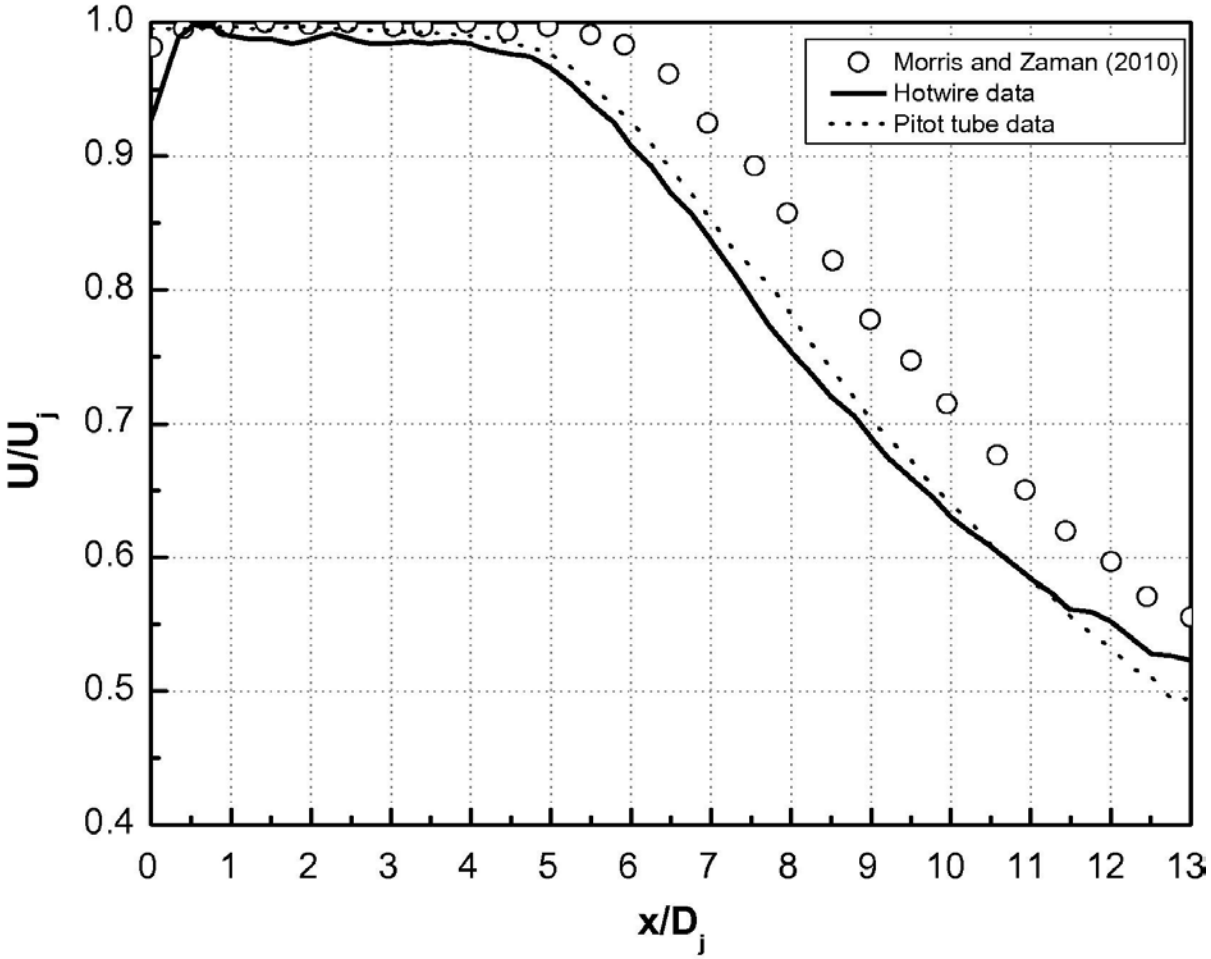

Fig. 13. Velocity distribution along the jet centerline axis for Mach 0.25. Velocity distribution along the jet centerline axis for Mach 0 Hot-wire; Velocity distribution along the jet centerline axis for Mach 0 Pitot-tube; ○ Morris and Zaman [16].

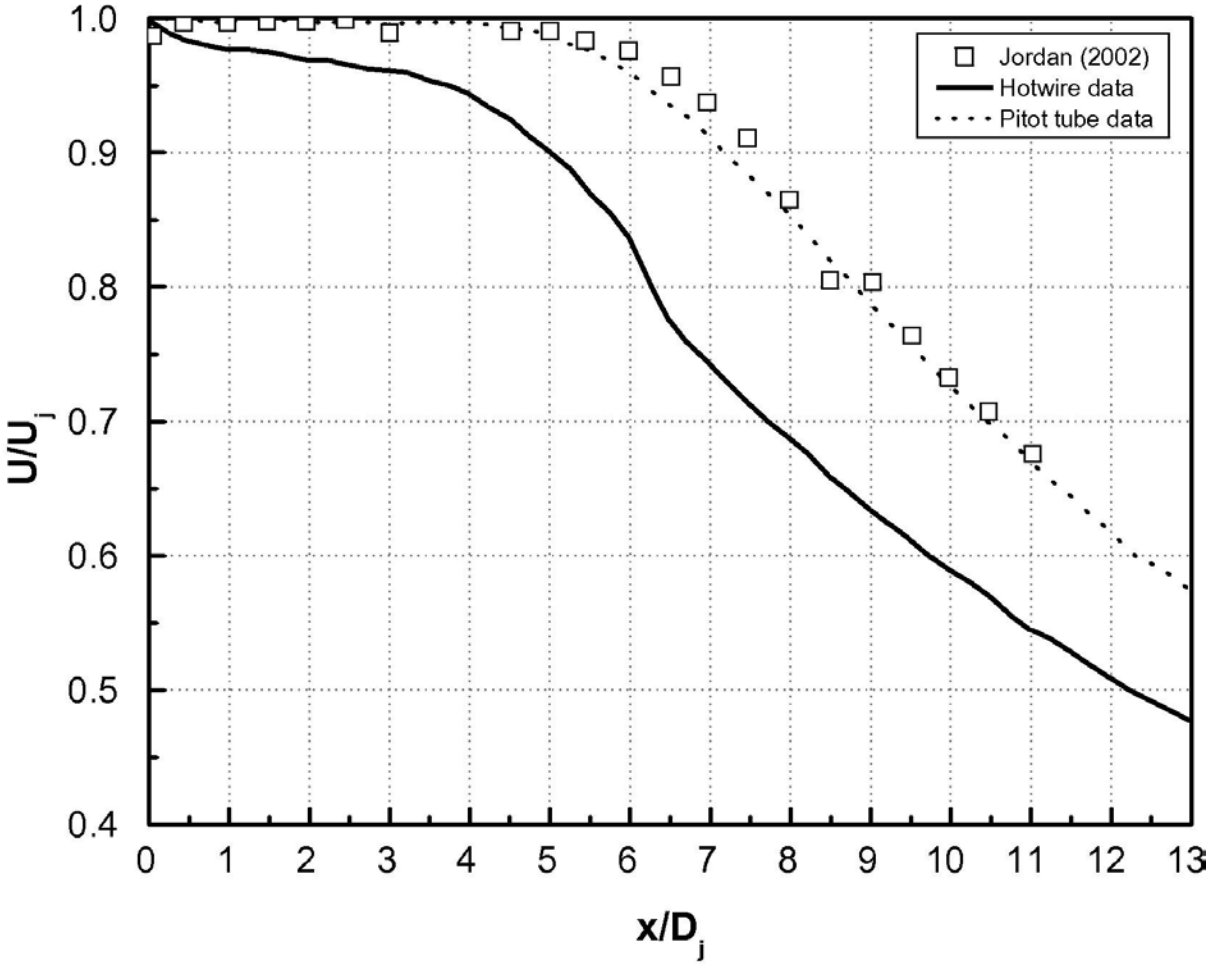

Fig. 14. Velocity distribution along the jet centerline axis for Mach 0.75. Velocity distribution along the jet centerline axis for Mach 0 Hot-wire; Velocity distribution along the jet centerline axis for Mach 0 Pitot-tube; □ Jordan [17].

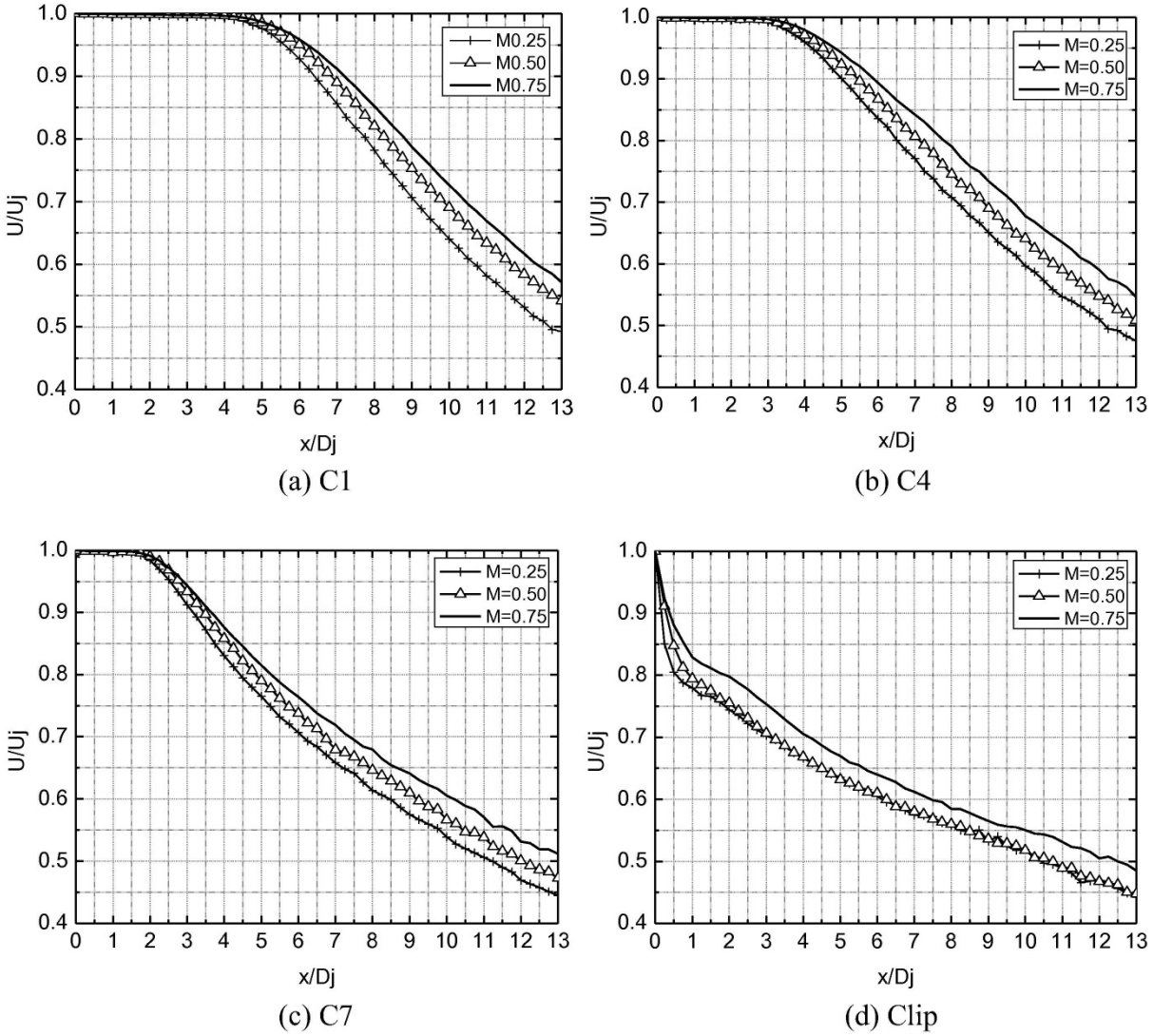

Fig. 15. Comparison of velocity profiles at different Mach numbers. Axial lines: (a) C1, (b) C4, (c) C7 and (d) Clip acquired with Pitot-tube. Comparison of velocity profiles at different Mach numbers Mach 0.25; Comparison of velocity profiles at different Mach numbers Mach 0.50; Comparison of velocity profiles at different Mach numbers Mach 0.75.

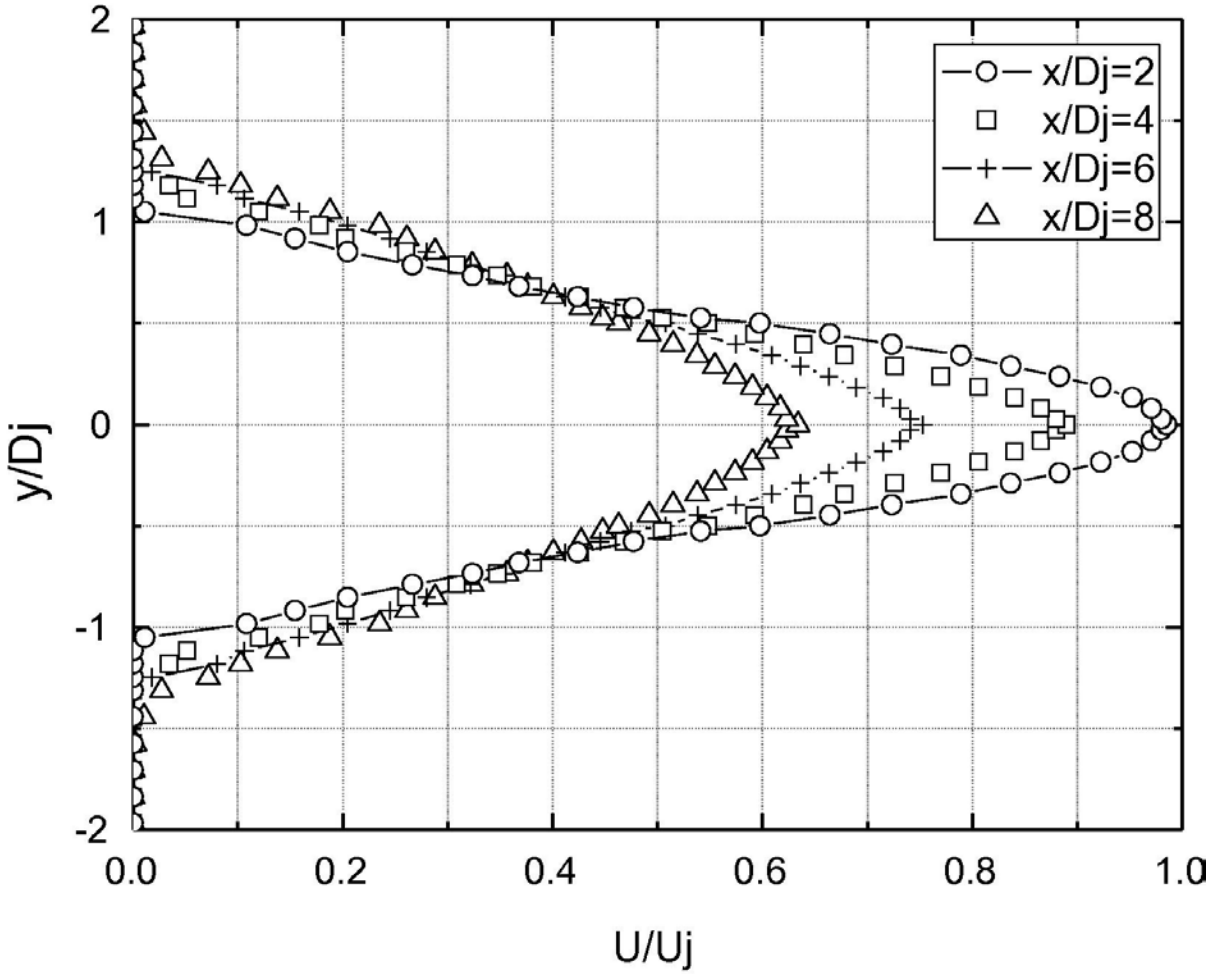

Fig. 16. Radial velocity profile of the jet at Mach 0.50 in function of the normalized velocity, obtained through Pitot-tube probe. -○- x/Dj = 2; □ x/Dj = 4; -+- x/Dj = 6; Δ x/Dj = 8.

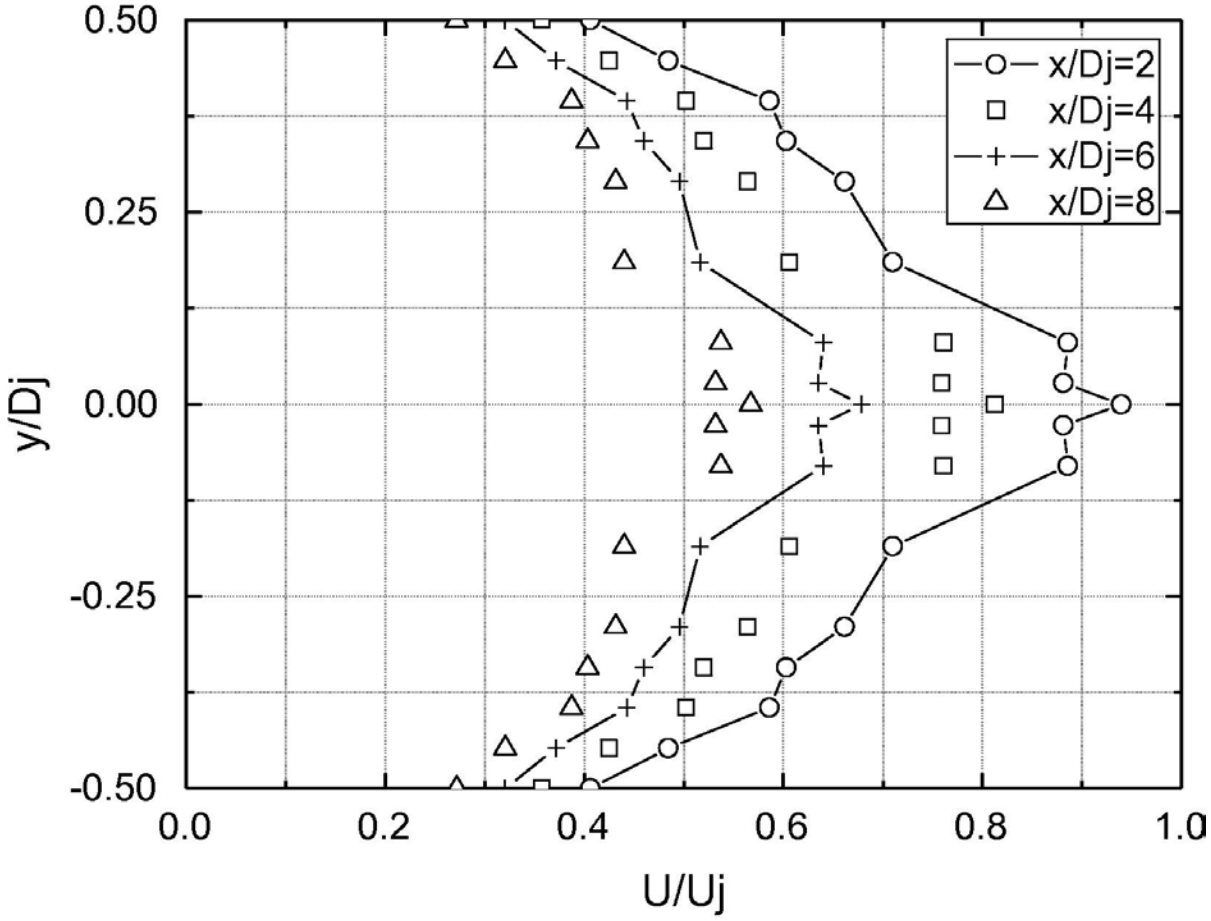

Fig. 17. Radial velocity profile of the jet at Mach 0.50 in function of the normalized velocity, obtained through hot-wire probe. -○- x/Dj = 2; □ x/Dj = 4; -+- x/Dj = 6; Δ x/Dj = 8.

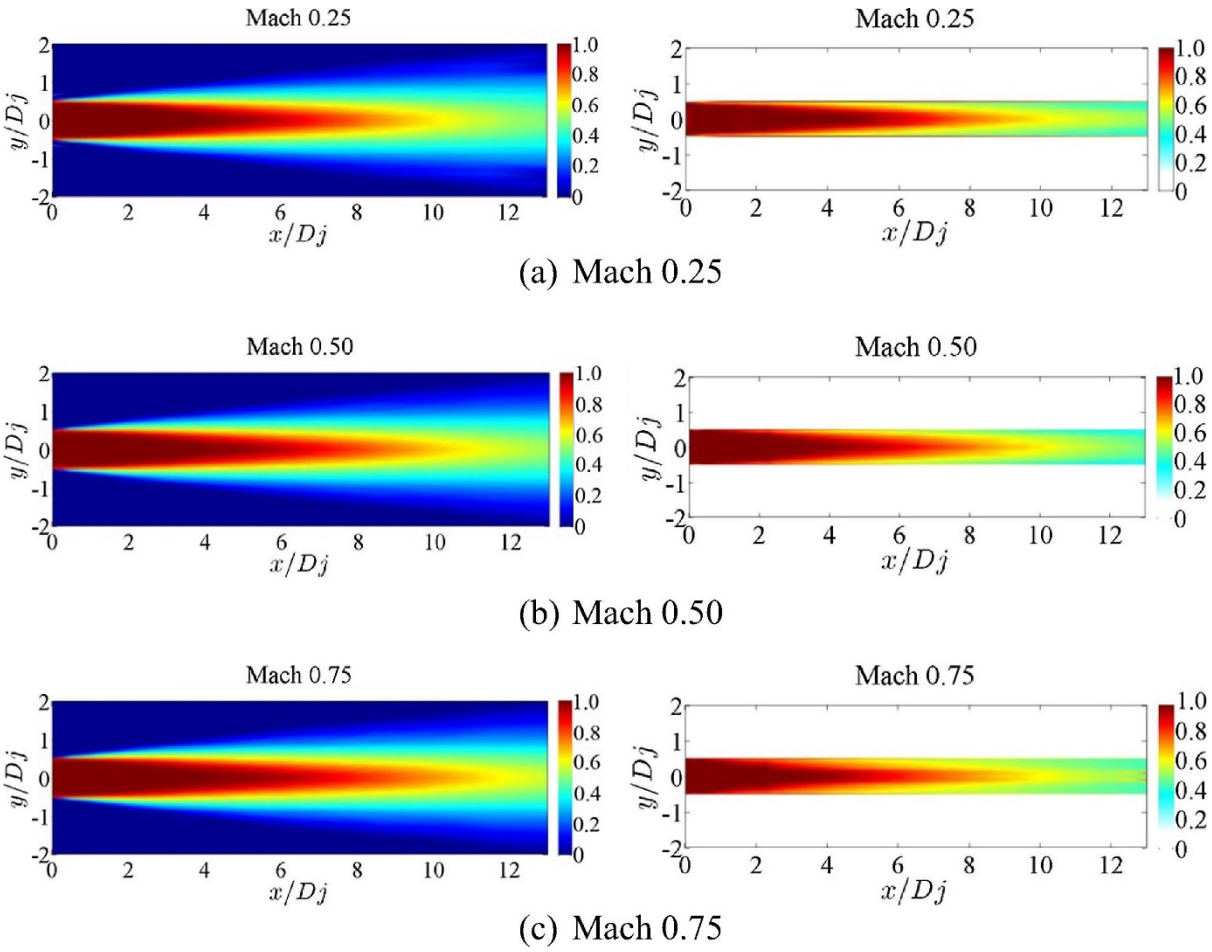

Fig. 18. Jet characterization with Pitot-tube and hot-wire probes, respectively: (a) Mach 0.25; (b) Mach 0.50; (c) Mach 0.75.

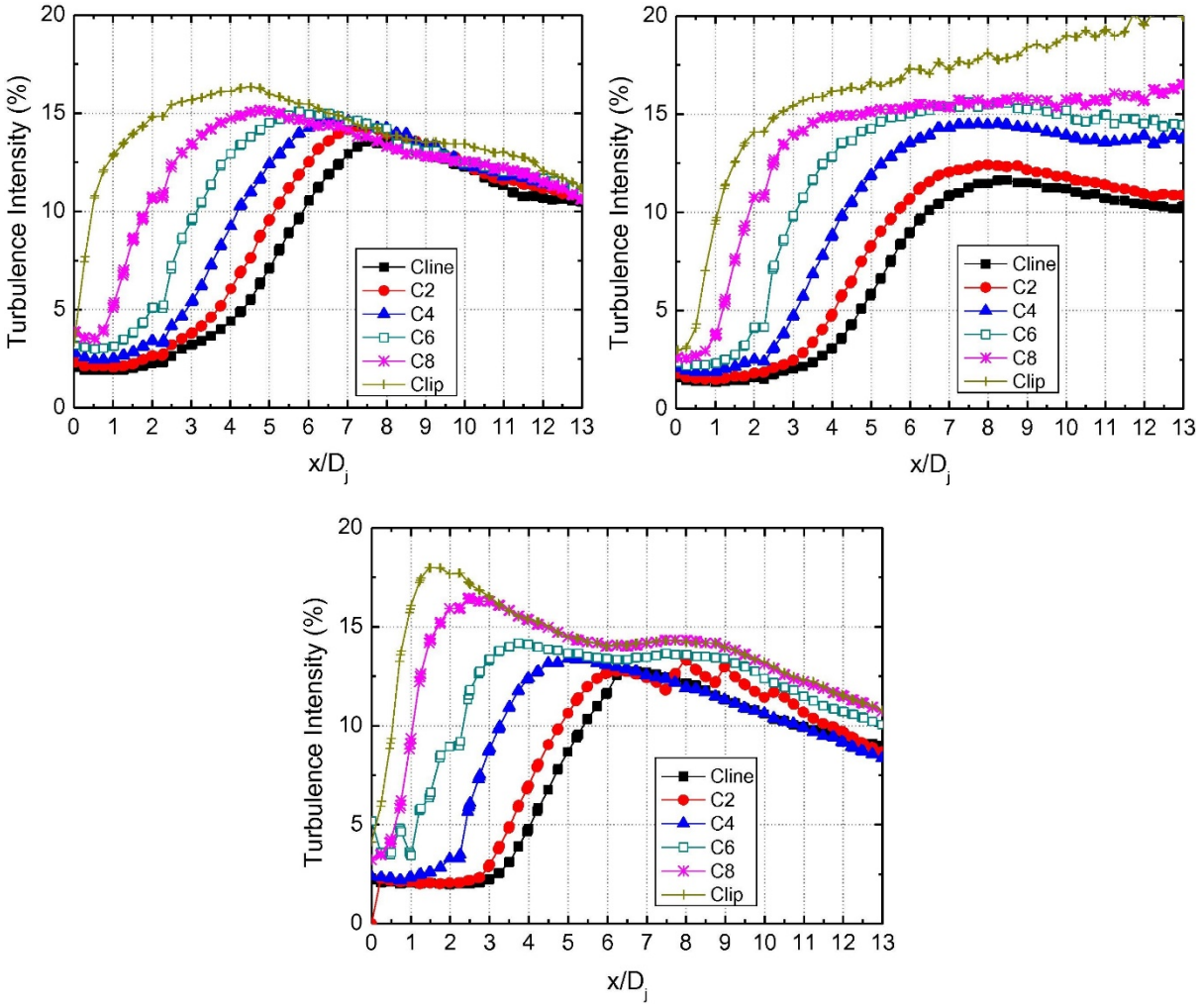

Fig. 19. Unsteadiness velocity distribution along the jet axis for different radial positions obtained through single hot-wire probes, Mach 0.25, 0.50 and 0.75, respectively.

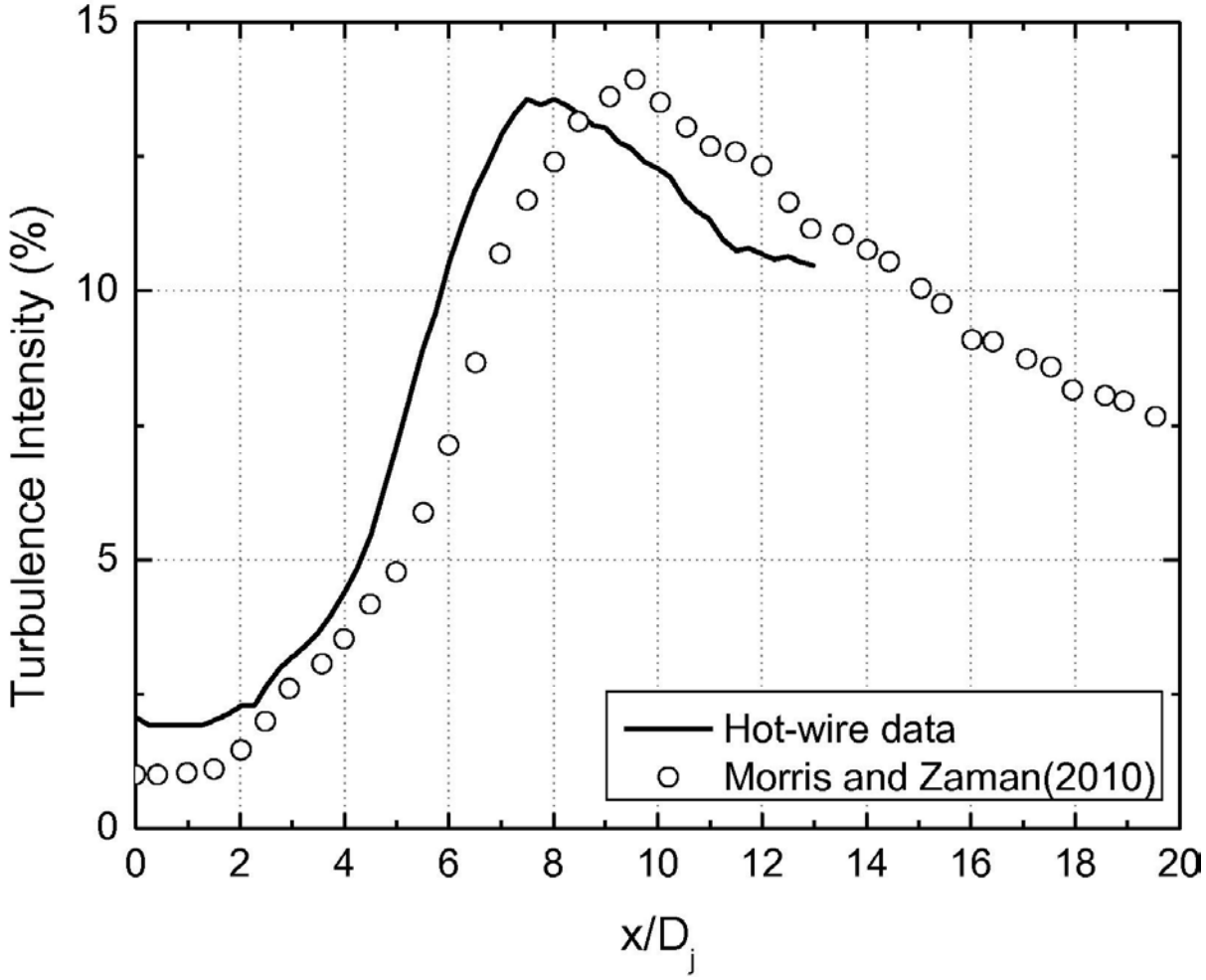

Fig. 20. Turbulence intensity along the jet axis (centerline) at Mach 0.25.

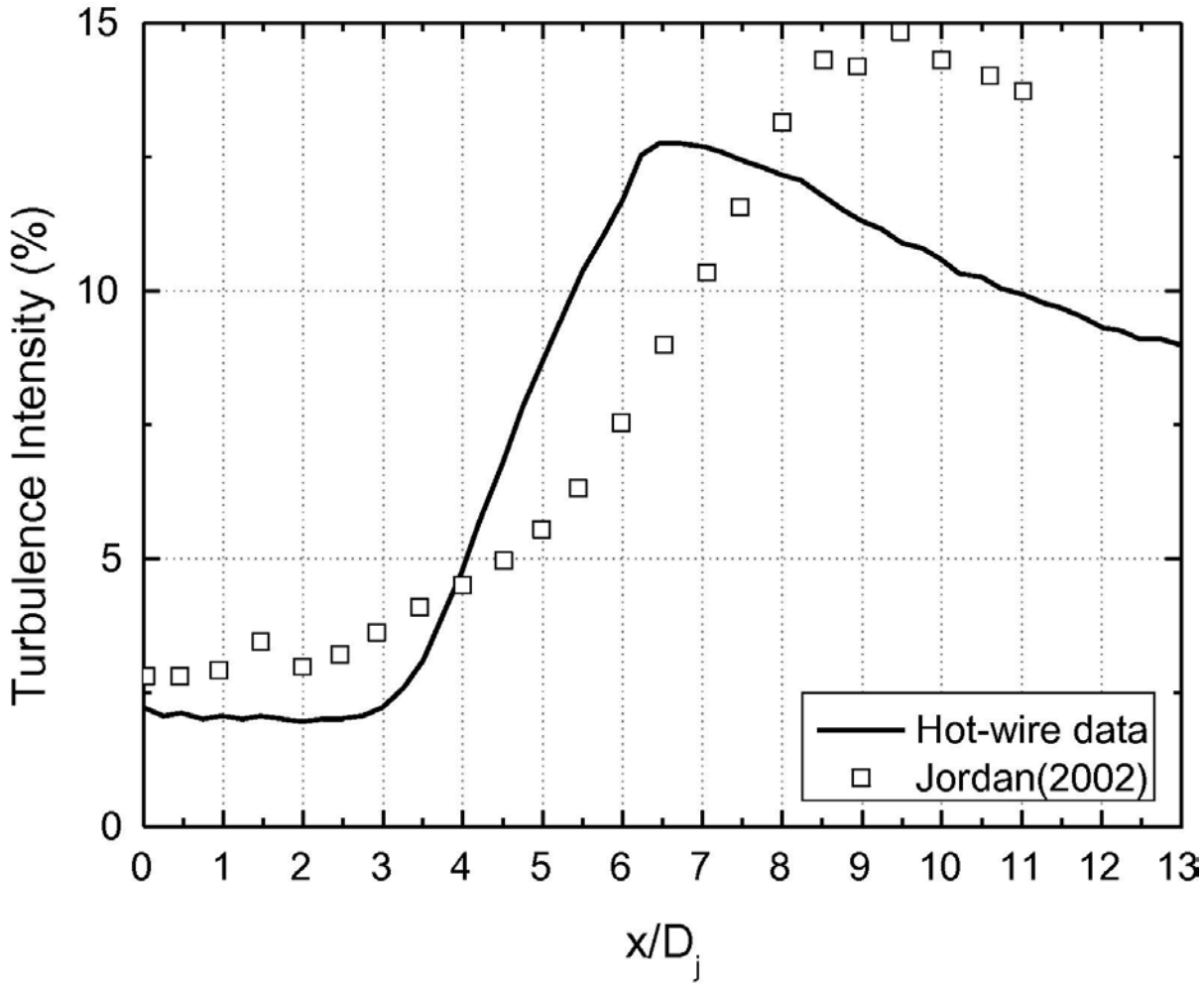

Fig. 21. Turbulence intensity along the jet axis (centerline) at Mach 0.75.

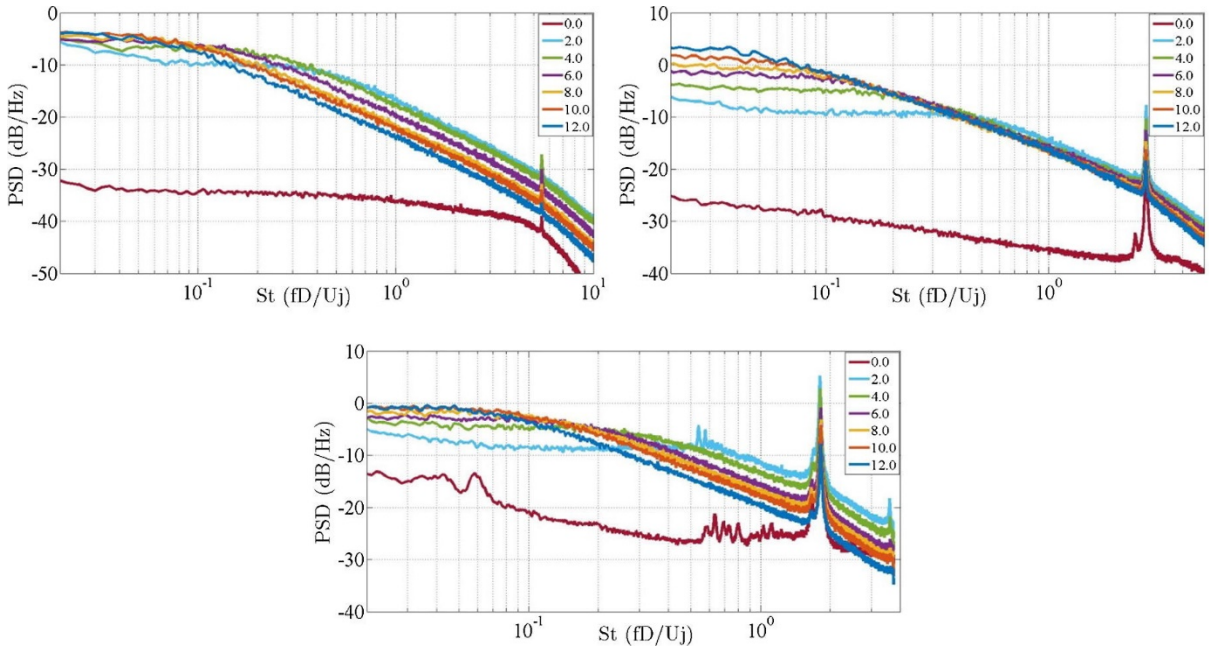

Fig. 22. Power spectral density in measurements at Mach numbers 0.25 (a), 0.50 (b) and 0.75 (b) at locations x/Dj = 0, 2, 4, 6, 8, 10 and 12.

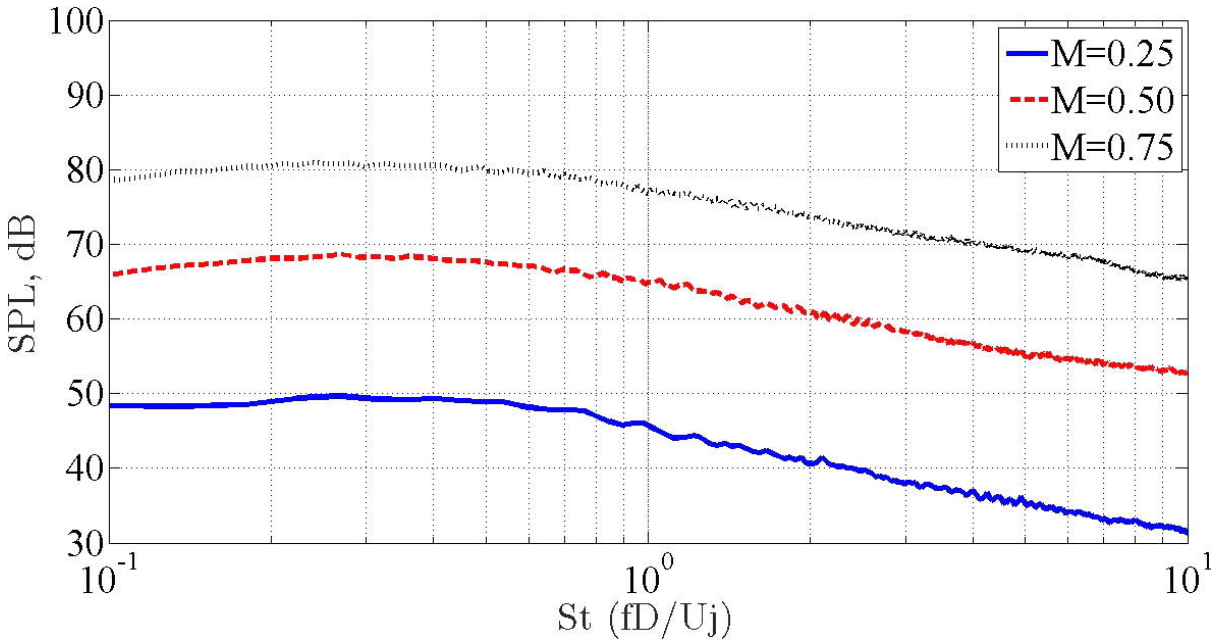

Fig. 23. Sound Pressure Level for different velocities at θ = 90°.

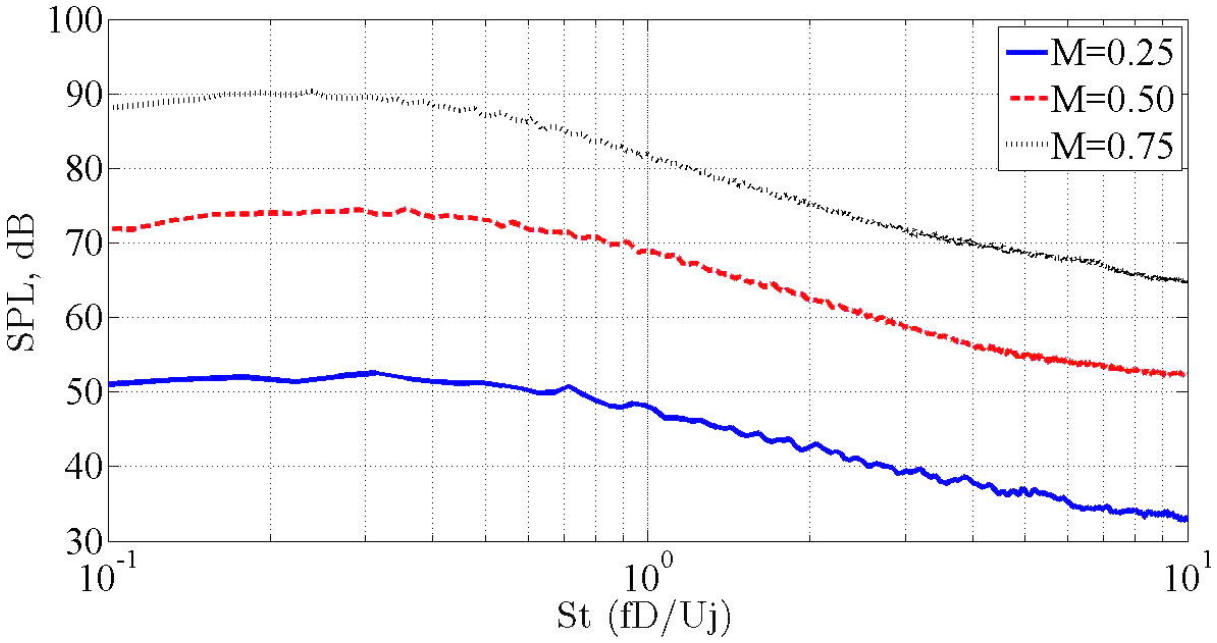

Fig. 24. Sound Pressure Level for different velocities at θ = 40°.

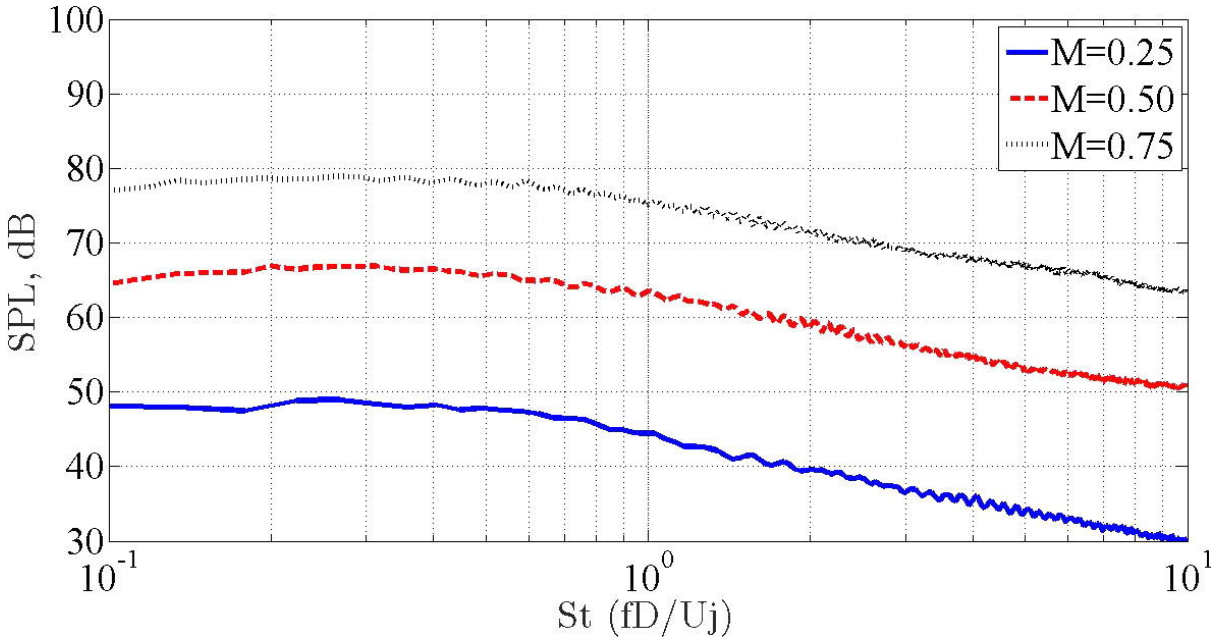

Fig. 25. Sound Pressure Level for different velocities at θ = 110°.

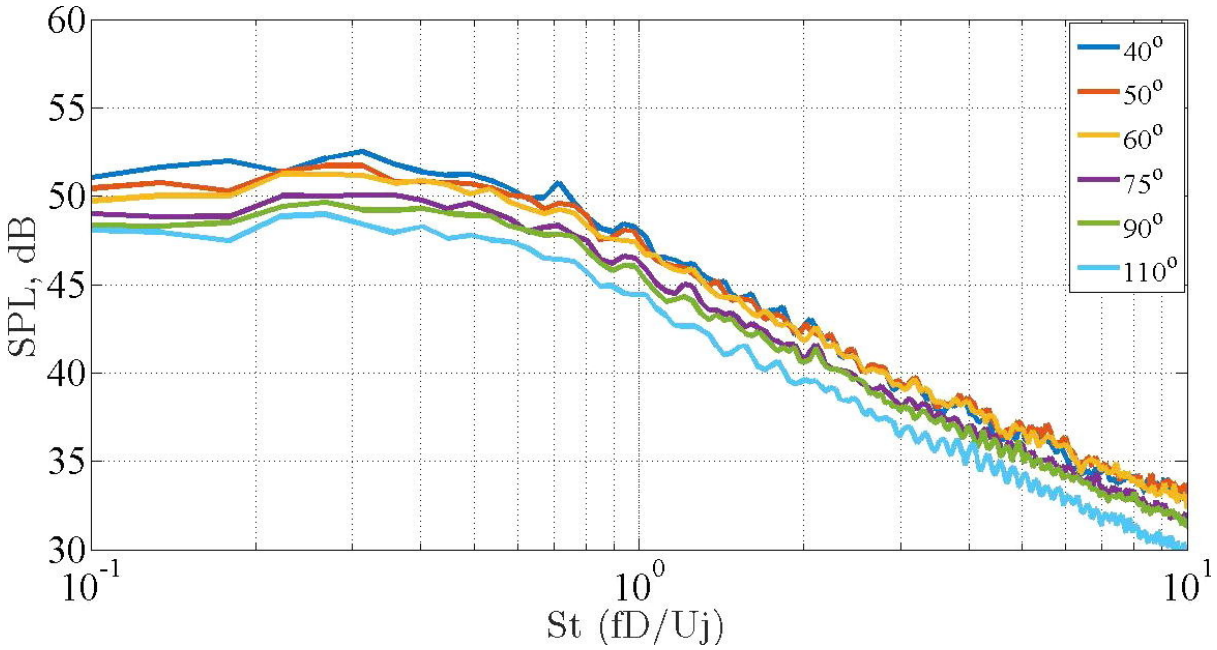

Fig. 26. Sound pressure level for Mach number 0.25 at six observer angles.

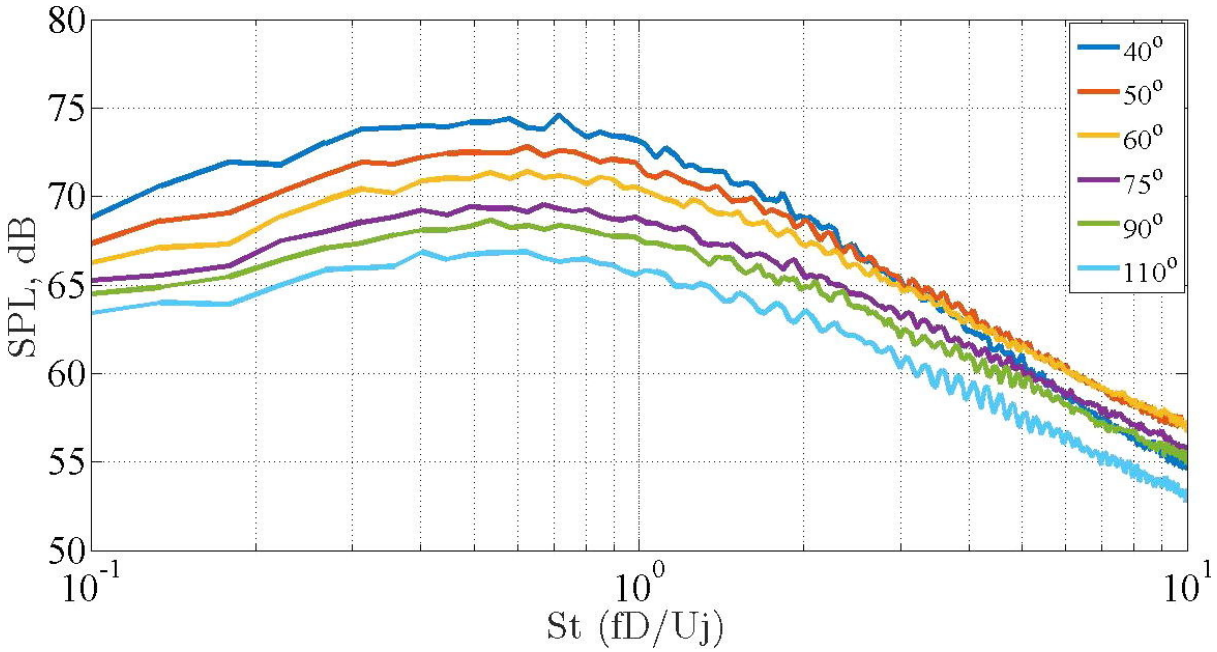

Fig. 27. Sound pressure level for Mach number 0.50 at six observer angles.

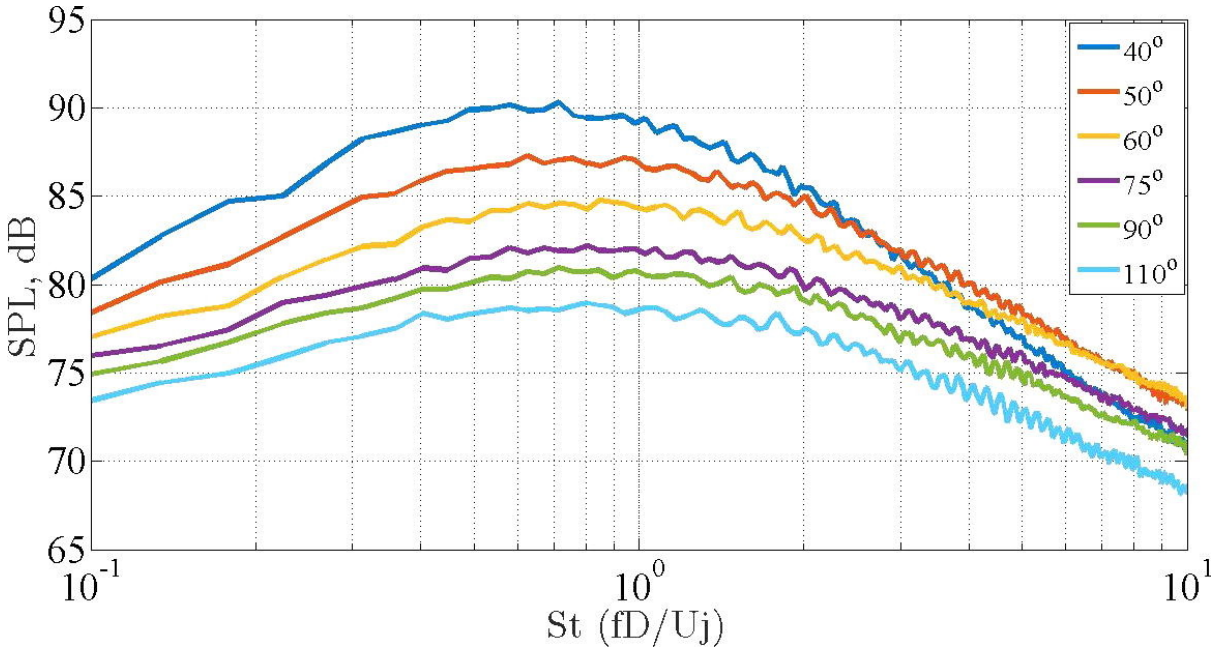

Fig. 28. Sound pressure level for Mach number 0.75 at six observer angles.

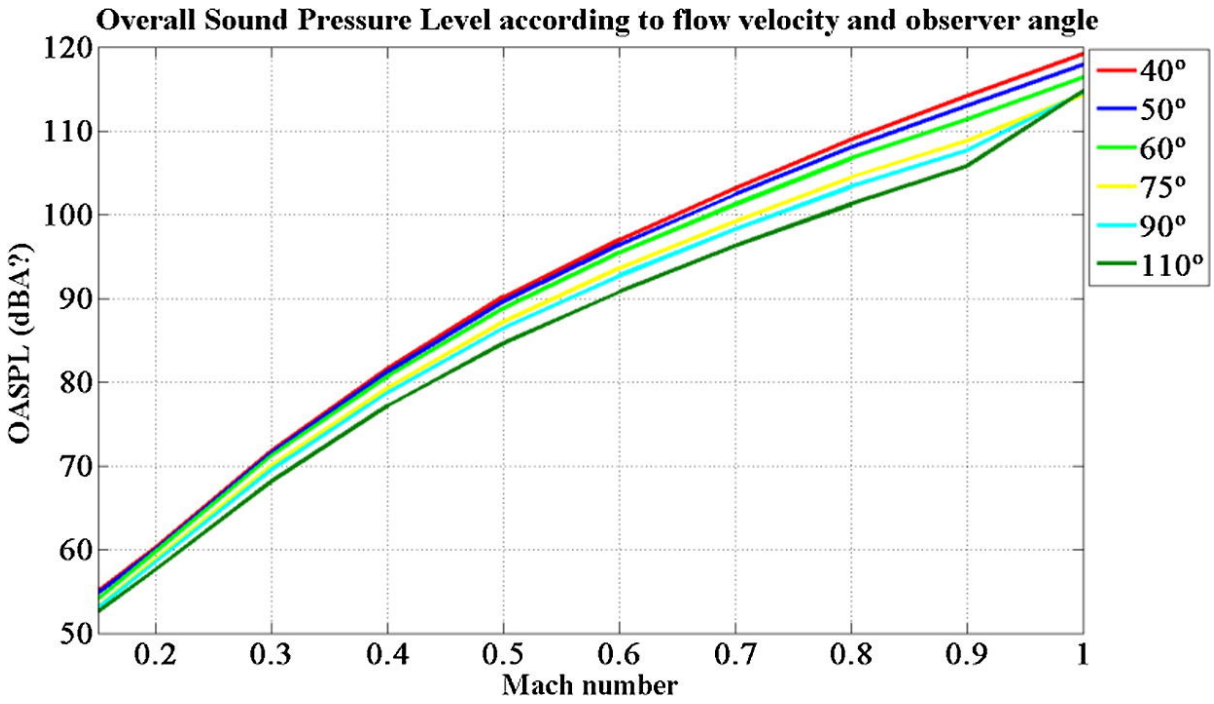

Fig. 29. The OASPL calculated vs Mach number in the range of observer angles.